Acidification of the Nordic Seas

Filippa Fransner[1], Friederike Fröb[1,2], Jerry Tjiputra[3], Nadine Goris[3], Siv K. Lauvset[3], Ingunn Skjelvan[3], Emil Jeansson[3], Abdirahman Omar[3], Melissa Chierici[4], Elizabeth Jones[4], Agneta Fransson[5], Sólveig R. Ólafsdóttir[6], Truls Johannessen[1], and Are Olsen[1]

[1]Geophysical Institute, University of Bergen, and Bjerknes Centre for Climate Research, Bergen, Norway
[2]Max Planck Institute for Meteorology, Hamburg, Germany
[3]NORCE Norwegian Research Centre, Bjerknes Centre for Climate Research, Bergen, Norway
[4]Institute of Marine Research, Fram Centre, Tromsø, Norway
[5] Norwegian Polar Institute, Tromsø, Norway
[6]Marine and Freshwater Research Institute, Reykjavík, Iceland

Correspondence: Filippa Fransner (filippa.fransner@uib.no)

Abstract.

Due to low calcium carbonate saturation states, and deep winter mixing that brings anthropogenic carbon to the deep ocean, the Nordic Seas and their cold-water corals are vulnerable to ocean acidification. Here, we present a detailed investigation of changes in pH and aragonite saturation in the Nordic Seas from pre-industrial times to 2100, by using *in situ* observations, gridded climatological data, and projections for three different future scenarios with the Norwegian Earth System Model (NorESM1-ME).

During the period of regular ocean biogeochemistry observations from 1981-2019 the pH decreased with rates of 2-3 10^{-3} yr^{-1} in the upper 200 m of the Nordic Seas. In some regions, the pH decrease can be detected down to 2000 m depth. This resulted in a decrease of the aragonite saturation state, which now is close to undersaturation in the depth layer of 1000-2000 m. The model simulations suggest the pH of the Nordic Seas to decrease at an overall faster rate than the global ocean from preindustrial to 2100, bringing the Nordic Seas pH closer to the global average. In the esmRCP8.5 scenario, the whole water column is projected to be undersaturated with respect to aragonite at the end of the 21st century, endangering all cold water corals of the Nordic Seas. In the esmRCP4.5 scenario, the deepest cold water coral reefs are projected to be exposed to undersaturation. Exposure of all cold-water corals to corrosive waters can only be avoided with marginal under the esmRCP2.6 scenario.

Over all time scales, the main driver of the pH drop is the increase in dissolved inorganic carbon, followed by temperature. Thermodynamic salinity effects are of secondary importance. We find substantial changes in alkalinity and dissolved inorganic carbon as a result of the salinification of the Atlantic Water during all time periods, and as a result of an increased freshwater export in polar waters in past and future scenarios. However, the net impact of this change in freshwater content on pH is negligible, as the effect of the freshwater-driven alkalinity change is cancelled out by the effect of the freshwater-driven change in dissolved inorganic carbon that has an opposite effect on pH. The effect of the salinification in the western Nordic Seas, and the increasing freshwater export in the eastern Nordic Seas, on pH are therefore negligible.

1 Introduction

Since 1850, human activities have released 650 $\pm$ 65 Gt of carbon to the atmosphere, of which about 25% has been taken up by the oceans (Friedlingstein et al., 2020) where it has been added to the pool of dissolved inorganic carbon (C_T). The increasing C_T has resulted in surface seawater pH decline of approximately 0.1 in the global ocean from pre-industrial to present-days, which corresponds to an approximately 30% increase in hydrogen ion (H^+) concentration (e.g., Doney et al., 2009; Gattuso and Hansson, 2011; Jiang et al., 2019). Furthermore, the decreasing pH also causes a reduction in the calcium carbonate ($CaCO_3$) saturation state (Ω). It hence poses a serious threat to marine organisms that have shells or structures consisting of $CaCO_3$, such as pteropods and corals (Guinotte et al., 2006; Turley et al., 2007; Manno et al., 2017; Doney et al., 2020; Doo et al., 2020). Depending on the CO_2 concentration pathway, future projections suggest further reductions of surface ocean pH of 0.1-0.3 from the 1990s until the end of the 21st century (Bopp et al., 2013). While global average acidification rates for surface waters, both from pre-industrial times to present-day and as projected for the future, are investigated in several studies (e.g. Caldeira and Wickett, 2003; Raven et al., 2005; Kwiatkowski et al., 2020), less is known about acidification rates on regional scales, especially below the surface.

The Nordic Seas, comprised of the Greenland, Iceland and Norwegian seas (Fig. 1) and bounded by the Fram Strait in the north, the Barents Sea Opening to the northeast and the Greenland-Scotland Ridge in the south, are of particular interest when it comes to ocean acidification due to their specific dynamic, biogeochemical and ecosystem characteristics. The surface circulation pattern of the Nordic Seas (e.g. Blindheim and Østerhus, 2013; Våge et al., 2013) is dominated by the relatively warm, saline Atlantic waters that flow northward as the Norwegian Atlantic Current in the east, mainly constrained to the Norwegian Sea, and relatively cold and fresh waters of Arctic origin flowing southward as the East Greenland Current in the west. In the Greenland and Iceland Seas, deep and intermediate water masses are formed through open-ocean convection (Våge et al., 2015; Brakstad et al., 2019). Some of these water masses ultimately overflow the Greenland-Scotland Ridge and feed into the North Atlantic Deep Water helping to sustain the lower limb of the Atlantic Meridional Overturning Circulation (AMOC, Dickson and Brown, 1994; Våge et al., 2015; Chafik and Rossby, 2019). The surface water pCO_2 is generally lower than that of the atmosphere, making the Nordic Seas important sinks for atmospheric CO_2. This undersaturation results from several processes, including primary production, cooling of northward flowing Atlantic waters, and the inflow of pCO_2 undersaturated waters from the Arctic Ocean (Anderson and Olsen, 2002; Takahashi et al., 2002; Ólafsson et al., 2020b). Although the Nordic Seas are an overall sink for atmospheric CO_2, the direct uptake of anthropogenic CO_2 through air-sea CO_2 exchange is limited. Instead, there is a large advective supply of excess anthropogenic CO_2 from the south (Anderson and Olsen, 2002; Olsen et al., 2006; Jeansson et al., 2011) that contributes to the acidification. Part of the anthropogenic CO_2 that enters the Nordic Sea's surface waters is brought to deep waters through the deep water formation, from where it is slowly advected to the North Atlantic Ocean (Tjiputra et al., 2010; Perez et al., 2018). The deep reaching anthropogenic CO_2, in combination with the prevailing low temperatures that give low saturation states of $CaCO_3$ (Ólafsson et al., 2009; Skjelvan et al., 2014), make the cold-water coral reefs of the Nordic Seas particularly exposed to ocean acidification(Kutti et al., 2014).

There has been extensive research on changes in the carbonate system and pH in the Nordic Seas, facilitated by the many research and monitoring cruises in the area (e.g., Olsen et al., 2006; Ólafsson et al., 2009; Skjelvan et al., 2008; Chierici et al., 2012; Skjelvan et al., 2014; Jones et al., 2020; Skjelvan et al., 2021; Pérez et al., 2021). Between the 1980s and 2010s, the pH has been shown to decrease with rates of -0.0023 to -0.0041 y^{-1} in surface waters, which is greater than expected from the increase in atmospheric CO_2 alone (Ólafsson et al., 2009; Skjelvan et al., 2014). This is consistent with the many observations that have indicated a weakening of the pCO_2 undersaturation of the Nordic Seas surface waters, i.e., that surface ocean pCO_2 has risen faster than the atmospheric pCO_2 (Olsen et al., 2006; Skjelvan et al., 2008; Ólafsson et al., 2009), over the past decades. The future pH of the Nordic Seas have been assessed with different modelling approaches (Bellerby et al., 2005; Skogen et al., 2014, 2018). Bellerby et al. (2005) investigated the impact of climate change on the Nordic Seas CO_2 system under a doubling of the atmospheric CO_2 to a value of 735 ppm. It was done by combining observed relationships between the inorganic CO_2 system and temperature and salinity, with output of ocean physics from the Bergen Climate Model. They found the pH to decrease by about 0.3, with the largest decrease taking part in the polar waters of the eastern Nordic Seas. For the future scenario A1B (see Meehl et al., 2007), which assumes approximately 700ppm atmospheric CO_2 by the year 2100, Skogen et al. (2014) found that the pH of the Nordic Seas surface waters decreases by 0.19 between 2000 and 2065, and that the aragonite saturation horizon shoals by 1200 m. They estimated C_T to be the overall driver of this acidification. Skogen et al. (2018) looked into future changes in the Nordic Seas biogeochemistry under the Representative Concentration Pathway 4.5 (RCP4.5) scenario, a stabilization future scenario used within Climate Model Intercomparison Project Phase 5 (CMIP5 Taylor et al., 2012), and found the surface pH to drop by 0.18 between 1995 and 2070.

All the studies mentioned above have been focusing on selected periods of time and scenarios, using specific datasets. There is, to our knowledge, no work assessing pH changes and their drivers from the pre-industrial until the end of the 21st century, under different scenarios, using both observational and modelling data, and that provides a detailed regional perspective on the various drivers. In this study, we fill this gap by examining past, present-day, and projected future changes in pH and aragonite saturation in the Nordic Seas, over the full water column and in different regions, by using the best available information for the various time periods. This includes a combination of *in situ* observations, gridded climatological data, and Earth System Model (ESM) projections for different future scenarios.

2 Drivers of pH and saturation states - Theoretical Background

The rising atmospheric CO_2 concentration results in a flux of CO_2 from the atmosphere into the ocean. In the ocean CO_2 reacts with water to form carbonic acid (H_2CO_3), which then dissociates into bicarbonate (HCO_3^-) and hydrogen ions (H^+). A large part of the resulting H^+ is neutralized by carbonate ions (CO_3^{2-}) that have been supplied to the ocean by the weathering of

carbonate and silicious minerals. Together, this forms the following equilibria:

$$CO_2 + H_2O \rightleftharpoons H_2CO_3 \quad (1)$$

$$H_2CO_3 \rightleftharpoons HCO_3^- + H^+ \quad (2)$$

$$CO_3^{-2} + H^+ \rightleftharpoons HCO_3^- \quad (3)$$

Combined, the concentration of CO_2, H_2CO_3, HCO_3^-, and CO_3^{2-}, constitute the concentration of dissolved inorganic carbon (C_T). In seawater, approximately 90% of C_T exists in the form of HCO_3^-, 9% as CO_3^{2-} and 1% as CO_2.

As seen from Equations 1 - 3, the dissolution of CO_2 in seawater results in an increase in H^+ concentration, which leads to a decrease in pH. On total scale, pH is defined as:

$$pH = -log_{10}([H^+] + [HSO_4^-]) \quad (4)$$

where HSO_4^- is sulphate. Apart from C_T, pH is influenced by temperature, salinity, and total alkalinity (A_T). A_T is mostly determined by HCO_3^- and CO_3^{2-} (carbonate alkalinity). Temperature and salinity affect pH by altering the dissociation constants and thus the partitioning of C_T between its different constituents. The relation between C_T and A_T influences pH by affecting the buffer capacity of seawater. The qualitative, direct effects of an increase in each property are shown in Table 1. Note that this Table does not consider indirect effects on pH, for example from the change in air-sea fluxes that will follow from e.g., a temperature driven pCO_2 change (e.g. Jiang et al., 2019; Wu et al., 2019).

Table 1. Direction of direct effects of an increase in temperature, salinity, C_T and A_T on pH and Ω.

Driver	pH	Ω
Temperature	-	+
Salinity	-	-
C_T	-	-
A_T	+	+

Equations 1 to 3 show that an increase in anthropogenic CO_2 and C_T results in a reduction in CO_3^{2-}. This affects the saturation state of $CaCO_3$ (Ω), defined as:

$$\Omega = \frac{[Ca^{2+}][CO_3^{2-}]}{K_{sp}}, \quad (5)$$

where K_{sp} is the solubility product. When Ω is less than one, the water becomes corrosive and $CaCO_3$ starts to dissolve. In seawater, the two most abundant forms of $CaCO_3$ are calcite and aragonite. The saturation state of aragonite (Ω_{Ar}) is lower than that of calcite (Ω_{Ca}) as aragonite is more soluble than calcite, equating to a higher K_{sp}.

The impact of C_T on the saturation state is seen in the spatial distribution of Ω in the surface ocean, which broadly follows temperature gradients (e.g. Orr, 2011; Jiang et al., 2019). The reason behind this temperature dependency is the higher

CO_2 solubility of colder waters. Consequently, cold waters have a relatively low Ω_{Ar} and Ω_{Ca} and are more vulnerable to acidification. Ω is also influenced by A_T, temperature and salinity, as shown in Table 1.

The sensitivity of pH and Ω to an anthropogenic CO_2 increase is dependent on the buffer capacity of the seawater (e.g. Sarmiento and Gruber, 2006; Orr, 2011). Waters with a higher buffer capacity, i.e., higher concentrations of CO_3^{2-}, have the capability of converting a larger fraction of the absorbed CO_2 into bicarbonate. A smaller fraction remains as dissolved CO_2, implying a smaller increase in the seawater pCO_2. These waters therefore have the capability of absorbing more CO_2 for any given increase in atmospheric pCO_2 (assuming a uniform increase in pCO_2 between water masses), which also implies a larger decline in $CaCO_3$ saturation state. pH is, on the contrary, decreasing more in waters with lower buffer capacity as they are less effective in neutralising carbonic acid.

3 Data

3.1 Observational data

As observational data, we used C_T, A_T, temperature, salinity, phosphate, and silicate data collected between 1981 and 2019 during dedicated research cruises, at two time-series stations, and in the framework of the Norwegian program "Monitoring ocean acidification in Norwegian waters". Sampling locations are shown in Fig. 1.

Data from 28 research cruises (Brewer et al., 2010; Anderson et al., 2013a, b; Anderson, 2013a, b; Bellerby and Smethie, 2013; Johannessen and Golmen, 2013; Johannessen, 2013a, b; Johannessen and Simonsen, 2013; Johannessen and Olsen, 2013; Johannessen et al., 2013c, a, b; Jones et al., 2013; Olsen et al., 2013; Olsen and Omar, 2013; Omar and Olsen, 2013; Omar and Skogseth, 2013; Omar, 2013; Pegler et al., 2013; Skjelvan et al., 2013; Wallace and Deming, 2014; Lauvset et al., 2016; Tanhua, 2017; Jeansson et al., 2018; Marcussen, 2018; Schauer et al., 2018) in the Nordic Seas were extracted from the GLODAPv2.2019 data product, which provides bias-corrected, cruise-based, interior ocean data (Olsen et al., 2019). The GLODAPv2 data product is considered consistent among cruises within 0.005 for salinity, 2% for silicate , 2% for phosphate, and 4 μmol kg^{-1} for both C_T and A_T (Olsen et al., 2019).

Time-series data are from Ocean Weather Station M in the Norwegian Sea, and from the Iceland Sea. The data from the Ocean Weather Station M, located at 66 °N and 2 °E, have been described in Skjelvan et al. (2008). At this station, sampling at 12 depth levels between surface and seabed (2100 m) was carried out each month between 2002 and 2009, and 4-6 times each year between 2010 and 2019. For these data, the uncertainty related to the measurements is 0.001 for salinity, 0.7 μmol kg^{-1} for silicate, 0.06 μmol kg^{-1} for phosphate, and 2 μmol kg^{-1} for C_T and A_T. The time-series station in the Iceland Sea, covering the period of 1985-2019, is situated at 68 °N and 12.67 °W. It is visited approximately 4 times a year and samples are taken at 10-20 depth levels between surface and seabed (1900 m). The uncertainty related to the measurements at this station is 0.005 for salinity, 2% for silicate, 2% for phosphate, and 4 μmol kg^{-1} for both C_T and A_T. These data have been described in Ólafsson et al. (2009).

The data from the program "Monitoring ocean acidification in Norwegian waters" were sampled in the full water column along repeated sections in the Nordic Seas in the period 2011-2019 (Chierici et al., 2012, 2013, 2014, 2015, 2016, 2017; Jones

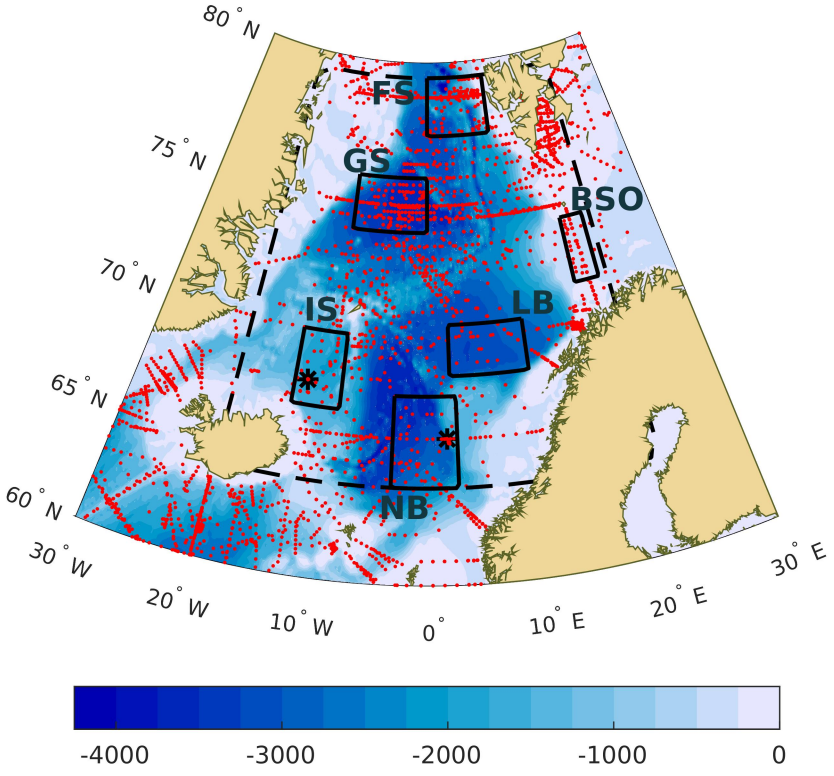

Figure 1. Map of the Nordic Seas with sampling locations (red). Also shown are the locations of the six regions where trends have been analyzed separately (rectangles), that is BSO: Barents Sea Opening; FS: eastern Fram Strait; GS: Greenland Sea; IS: Iceland Sea; LB: Lofoten Basin and NB: Norwegian Basin. The dashed line marks the borders of the area that we define as the Nordic Seas. The asterisk markers in the Norwegian Basin and the Iceland Sea show the positions of Ocean Weather station M and the Iceland Sea time-series station, respectively. The filled contours illustrate the bathymetry at 250 m intervals.

et al., 2018, 2019, 2020). The uncertainties related to the sampled data is 0.005 for salinity, 0.1 for silicate, 0.06 for phosphate, 2 μmol kg^{-1} for both C_T and A_T.

Data from the eastern Fram Strait were collected on cruises with RV Helmer Hansen within the CarbonBridge project, and on cruises with RV Lance (Chierici et al., 2019c) organized by the Norwegian Polar Institute.

Analytical methods for C_T and A_T, in all datasets described above (for GLODAP after the mid 1990s), follow Dickson et al. (2007) and the accuracy and precision is controlled by Certified Reference Materials (CRM), and by participation in international intercomparison studies (e.g. Bockmon and Dickson, 2015).

For estimates of atmospheric CO_2 change, we used the annual mean atmospheric CO_2 mole fraction (xCO_2) from the Mauna Loa updated records, downloaded from www.esrl.noaa.gov/gmd/ccgg/trends/. Although the absolute value of atmospheric xCO_2 varies with latitude, the growth rates are the same across the globe.

3.2 Gridded climatological data

Climatological distributions of pH and Ω_{Ar} were calculated from C_T, A_T, temperature, salinity, phosphate and silicate in the mapped GLODAPv2 data product (Lauvset et al., 2016). Pre-industrial pH was determined by subtracting the GLODAPv2 estimate of anthropogenic carbon from the mapped climatology of present (i.e., 2002) C_T (Lauvset et al., 2016). We assumed that the changes in the temperature, salinity and A_T of the Nordic Seas are of minor importance for changes in pH between pre-industrial times and present-day. The GLODAPv2 estimate of anthropogenic carbon have been calculated using the transit time distribution (TTD) approach. We note that we use the GLODAPv2 estimate of pre-industrial pH only for comparison with the ESM data, specifically in Fig. 4 (5.2).

3.3 Earth System Model data

For the estimates of past and future ocean acidification and saturation states under various climate scenarios, we primarily used output from the fully coupled Norwegian Earth System Model with interactive atmospheric CO_2 (NorESM1-ME, Bentsen et al., 2013; Tjiputra et al., 2013, 2016). NorESM1-ME includes the dynamical isopycnic vertical coordinate ocean model MICOM (Bleck and Smith, 1990) and the Hamburg Oceanic Carbon Cycle model (HAMOCC5, Maier-Reimer et al., 2005), adapted to the isopycnic ocean model framework. HAMOCC5 simulates lower trophic ecosystem processes up to the zooplankton level, including primary production, remineralization and predation, and full water column inorganic carbon chemistry. For our assessment, we utilised emission-driven historical simulations for the period from 1850 to 2005 and future scenarios simulations for the period from 2006 to 2100, with focus on RCP's 2.6, 4.5 and 8.5 (RCP2.6, RCP4.5, and RCP8.5; Meinshausen et al., 2011; van Vuuren et al., 2011a). RCP2.6 represents a mitigation scenario, RCP4.5 a stabilization scenario and RCP8.5 a high-emission scenario. For the emission-driven runs used here, the corresponding scenarios are named esmRCP2.6, esmRCP4.5 and esmRCP8.5. Because the emission-driven scenarios prognostically simulate the atmospheric CO_2 concentration, it normally deviates from the prescribed concentrations in the concentration-driven scenarios (e.g. Friedlingstein et al., 2014). This is most critical for the historical scenario, where the prescribed atmospheric CO_2 follows the observed evolution. Here, deviations in the simulated atmospheric CO_2 might result in pH changes that differ from the actual pH change. The deviation in the simulated atmospheric CO_2 concentration in the emission-driven NorESM1-ME scenarios, from the prescribed one in the concentration-driven scenarios, and its effect on pH, is shown in the supplementary Table S1. Between 1850 and 2005, the model simulates an increase in the atmospheric CO_2 that is 14 ppm too strong, which results in a pH drop that exceeds the expected one by 0.01. This deviation is, however, one order of magnitude smaller than the actual pH change between 1850 and 2005, and has the same order of magnitude as the estimated uncertainty in both observational data (Table 2) and GLODAPv2 pre-industrial pH estimate in the Nordic Seas (Sect. 4.4). The impact of the historical atmospheric CO_2 deviations between emission driven and concentration driven on pH change in our results is therefore negligible. Prior to experiments, NorESM1-

ME has undergone an extended spin-up procedure (>1000 years). The changes in pH, in all considered depth layers, is minor (more than one order of magnitude less) in the preindustrial control simulation compared to the historical run and the future scenarios, indicating that the impact of model drift on our results is insignificant .

As a means of uncertainty assessment, we use the outputs from an ensemble of emission-driven ESMs that participated in CMIP5 (Taylor et al., 2012). We chose emission-driven rather than concentration-driven scenarios, as they include the feedback of the carbon cycle on the physical climate (Booth et al., 2013) and thus give a more comprehensive estimate of the effect of model-related uncertainties on climate projections, and in particular on atmospheric CO_2, ocean carbon uptake and ocean acidification. It is well known that the inter-model spread is larger in emission-driven scenarios than in concentration-driven ones (Booth et al., 2013; Friedlingstein et al., 2014). While NorESM1-ME outputs are available for low to high future emission scenarios, the CMIP5 data-portals only contains emission-driven ESM outputs for the high future emission scenario (esmRCP8.5). Our ESM-ensemble consists of all ESMs that participated in the experiment 'esmrcp85' and RCP8.5, and whose output is publicly available in one of the CMIP5 data portals and contains all variables needed for our analysis. This results in an ensemble of 7 ESMs; 1) CESM1(BGC) (The Community Earth System Model, version 1 - Biogeochemistry, Long et al., 2013), 2) CanESM2 (second-generation Canadian earth system model, Arora et al., 2011)) , 3) GFDL-ESM2G (Geophysical Fluid Dynamics Laboratory Earth System Model with Modular Ocean Model, version 4 component, Dunne et al. 2013a; 2013b), 4) GFDL-ESM2M (Geophysical Fluid Dynamics Laboratory Earth System Model with Generalized Ocean Layer Dynamics (GOLD) component, Dunne et al. 2013a; 2013b), 5) IPSL-CM5A-LR (L'Institut Pierre-Simon Laplace Coupled Model, version 5A, low resolution, Dufresne et al., 2013), 6) MPI-ESM-LR (Max Planck Institute Earth System Model, low resolution, Giorgetta et al., 2013), and 7) MRI-ESM1 (Meteorological Research Institute-Earth System Model v1, Yukimoto et al., 2011). Both for NorESM1-ME and our model ensemble, we only investigate one realisation of each scenario.

3.4 Cold-water coral positions

To estimate the potential impact of the Nordic Seas acidification on cold-water corals, we used habitat positions in longitude and latitude from EMODnet Seabed Habitats (www.emodnet-seabedhabitats.eu) together with information on depth from ETOPO1 (NOAA National Geophysical Data Center, 2020).

4 Methods

4.1 Spatial drivers of pH and saturation states

To identify drivers of observed spatial variability of surface pH and Ω_{Ar}, we calculated pH and Ω_{Ar} by using spatially varying GLODAPv2 climatologies of specific drivers in Table 1, while keeping all other drivers constant (set to the spatial mean value of the Nordic Seas surface waters). Because the relation between C_T and A_T is a proxy for the buffer capacity, we decided to look at their combined effect on pH, meaning that both changes in C_T and A_T are included in the calculations. Their combined effect we from now on refer to as C_T+A_T. First, pH and Ω_{Ar} were calculated with temperature being the only spatially varying

climatology (pH(T), Ω_{Ar}(T)). Thereafter, we used spatially varying temperature, C_T and A_T climatologies to calculate pH(T, C_T, A_T) and Ω_{Ar}(T, C_T, A_T). Finally, the salinity variability was added to estimate pH(T, C_T, A_T,S) and Ω_{Ar}(T, C_T, A_T, S). To estimate the constribution of each driver, the pH and Ω_{Ar} fields calculated with the different spatially varying drivers were thereafter correlated with the actual pH and Ω_{Ar} of the Nordic Seas.

4.2 Temporal drivers of pH change

4.2.1 Present-day observational change

Measurements of temperature, salinity, C_T, and A_T (Figs. S1-S4), phosphate, and silicate from the data sets described in Sect. 3.1 were used to calculate pH and Ω_{Ar}, using CO2SYS for MATLAB (Lewis and Wallace, 1998; van Heuven et al., 2011). pH was calculated on total scale at in situ pressure and temperature. Wherever nutrient data were missing, silicate and phosphate concentrations were set to 5 μmol kg^{-1} and 1 μmol kg^{-1}, respectively, which are representative values for the Nordic Seas. For the CO2SYS calculations, the dissociation constants of Lueker et al. (2000), the bisulfate dissociation constant of Dickson (1990) and the borate-to-salinity ratio of Uppström (1974) were used. This ratio has recently been shown to be suitable for the western Nordic Seas (Ólafsson et al., 2020a).

Present-day trends (1981-2019) in pH, and Ω_{Ar} were determined for six different regions in the Nordic Seas: the Norwegian Basin (NB), the Lofoten Basin (LB), the Barents Sea Opening (BSO), eastern Fram Strait (FS), the Greenland Sea (GS) and the Iceland Sea (IS) (Fig. 1). These regions were chosen based on the data-availability, being centered around stations and sections where repeated measurements are taken, but also to get a representation of the main surface water masses of the Nordic Seas. In the surface, the Norwegian Basin, Lofoten Basin, and Barents Sea Opening are influenced by relatively warm and salty northward flowing Atlantic Water, while the Greenland and Iceland Seas are influenced by relatively cold and fresh southward flowing polar waters. As the Fram Strait surface is influenced by Atlantic and polar waters, we constrain the Fram Strait box to the east (hereinafter referred to as eastern Fram Strait) to ensure that it mostly represents Atlantic Waters. The geographical range of each regional box is kept small so that aliasing effects of latitudinal and longitudinal gradients are minimized.

Regional trends were computed from annual means for five different depth intervals (0-200, 200-500, 500-1000, 1000-2000, and 2000-4000 m) using linear regression. The relatively thick upper layer was chosen to keep all depths influenced by the seasonal cycle in one layer, that is, to minimize the number of layers where the trends may be affected by seasonal undersampling. As the winter mixed layer reaches approximately 200 m (e.g. Skjelvan et al., 2008), this depth sets the approximate lower limit for the impact of seasonal variations. The significance of the trends (at 95% confidence level), were determined from the p-value of the t-statistic (as implemented in MATLAB's fitlm function). For the comparison of trends, 95% confidence intervals of the slopes were determined by the use of the Wald method (as implemented in MATLAB's fitlm and coefCI functions).

The observed long-term changes in pH were decomposed into contributions from changes in temperature (T), salinity (S), C_T and A_T (Figs. S1-S4, and Tables S2-S5), following the procedure of Lauvset et al. (2015). First, the effect of each of these processes on the CO_2 fugacity (fCO_2) is determined following Takahashi et al. (1993):

$$\frac{dfCO_2}{dt} = \frac{\partial fCO_2}{\partial T}\frac{dT}{dt} + \frac{\partial fCO_2}{\partial S}\frac{dS}{dt} + \frac{\partial fCO_2}{\partial C_T}\frac{dC_T}{dt} + \frac{\partial fCO_2}{\partial A_T}\frac{dA_T}{dt} \tag{6}$$

The long-term mean values for the sensitivities (the fCO_2 partial derivatives) were approximated as in Fröb et al. (2019). Changes in A_T and C_T are driven by biogeochemical processes, transport, mixing and dilution or concentration by freshwater fluxes, which is in direct proportion to the dilution or concentration of salinity. The freshwater-effect can be separated by introducing salinity-normalized C_T (sC_T) and A_T (sA_T) (Keeling et al., 2004; Lovenduski et al., 2007):

$$sC_T = \frac{S_0}{S}(C_T - C_0) + C_0; \qquad sA_T = \frac{S_0}{S}(A_T - A_0) + A_0 \tag{7}$$

Here we set S_0 to 35 (Friis et al., 2003) and used the intercept of Eq. 6 and 7 in Nondal et al. (2009) as the non-zero freshwater end-member (A_0 and C_0). Substituting A_T and C_T in Eq. 6 by Eqs. 7 yields:

$$\frac{\partial fCO_2}{\partial C_T}\frac{dC_T}{dt} = \frac{sC_T - C_0}{S_0}\frac{\partial fCO_2}{\partial C_T}\frac{dS}{dt} + \frac{S}{S_0}\frac{\partial fCO_2}{\partial C_T}\frac{dsC_T}{dt} \tag{8}$$

$$\frac{\partial fCO_2}{\partial A_T}\frac{dA_T}{dt} = \frac{sA_T - A_0}{S_0}\frac{\partial fCO_2}{\partial A_T}\frac{dS}{dt} + \frac{S}{S_0}\frac{\partial fCO_2}{\partial A_T}\frac{dsA_T}{dt} \tag{9}$$

Subsequently, the magnitude of each fCO_2 driver is converted to $[H^+]$ by using Henry's law ($[CO_2] = k_0 \times fCO_2$) and the expression for $d[H^+]/d[CO_2]$ from equation 1.5.87 (Zeebe and Wolf-Gladrow, 2001):

$$\frac{d[H^+]}{dt} = \frac{d[H^+]}{d[CO_2]}\frac{k_0 \times dfCO_2}{dt} \tag{10}$$

Finally, H^+ in equation 10 was converted to pH by acknowledging that $dpH = -([H^+]\ln(10))^{-1}d[H^+]$. Here we consider the sulphate in Eq. 4 to be negligible, and did therefore not include it.

To control whether the observed pH changes are consistent with the changes in atmospheric CO_2, we additionally determined the pH change that can be expected in seawater where the pCO_2 perfectly tracks the atmospheric pCO_2 (pH_{perf}) for each region. This was achieved by adding the observed change in atmospheric xCO_2 to the local mean pCO_2 for the first year with observations, and then calculating the pH with CO2SYS with the local temperature, salinity, A_T, phosphate and silicate and their respective changes as inputs. We applied no corrections for water vapour and atmospheric pressure as the rates of change for xCO_2 and pCO_2 are proportional. Any deviation between observed pH change and pH_{perf} is a consequence of changes in seawater pCO_2 that are smaller/larger than in the atmosphere, i.e., a change in the air-sea pCO_2 difference.

4.2.2 Model- and observation-based past and future changes

As described in Sect. 2, the total change in pH and saturation states does not only depend on local changes in C_T, A_T, temperature, salinity, and nutrients, but also on the initial buffer capacity of the seawater. For the calculation of past and future pH changes, we use ESM data, which is usually biased, i.e., there is an offset between modelled fields and reality and this also holds for the buffer capacity. In particular, NorESM1-ME has high A_T and low C_T relative to observations in deep waters, leading to biased high pH (Fig. S5) and saturation states (not shown). To alleviate this bias in our analysis of past and future pH and Ω_{Ar}, we applied the modelled change of temperature, salinity, C_T, A_T, phosphate and silicate to the gridded GLODAPv2 climatology. Here, the modelled change between pre-industrial, present-day and future were calculated as differences between 10-year means; i.e., 1850-1859, 1996-2005 and 2090-2099, respectively. We note that we could not center our present-day 10-year mean around the year 2002 to which the GLODAPv2 climatology is normalized as the future scenarios start in 2006. After we obtained past and future states of the properties listed above, we calculated past and future pH, Ω_{Ar} and Ω_{Ca} in CO2SYS. Similar procedures have been used by Orr et al. (2005) and Jiang et al. (2019) to calculate future pH. Additionally, we used these data to calculate the drivers of past-to-present and present-day-to-future pH changes, following the methodology described in the previous section. Here we used a value of zero for the freshwater end members A_0 and C_0 as NorESM1-ME does not include any riverine input of A_T and C_T.

To estimate the impact of acidification on the cold-water corals of the Nordic Seas, we calculated the mean saturation state in our region east of 0 °E, and south of 64 °N, for P.I., present day and for the future under the esmRCP2.6, esmRCP4.5 and esmRCP8.5 scenarios. The exclusion of the western and northern parts was done to constrain the mean to the Atlantic Water where the cold-water corals are located. The saturation horizon was defined as the deepest vertical grid cell where $\Omega_{Ar} > 1$.

In order to facilitate a comparison with other model-based acidification studies, we have chosen to present the past and future changes for the surface ocean (i.e., 0 m) in Sect. 5.3 and 5.5. However, in Sect. 5.2, where the observed changes of the upper 200 m are put into perspective to past and future changes, we have calculated and presented the model mean over the upper 200 m.

4.3 pH or H^+ change?

In a recent publication, Fassbender et al. (2021) recommend to analyze changes in H^+ concentrations in addition to changes in pH, when comparing pH trends across water masses with different initial pH. The underlying reason is that a change in pH represents a relative change, and that it is possible to obtain the same pH changes across water masses with different change in H^+ concentration. We estimated the sensitivity of our results to the choice between pH and H^+ by plotting the change in H^+ concentration against the change in pH, for a given change in C_T at various initial pH (Fig. 2). The different initial pH were obtained by varying the C_T over A_T ratio, and the calculations were done with a temperature and salinity of 5°C and 35, respectively. For a given increase in C_T below 200 μmol kg^{-1}, we see that the relationship between the H^+ and pH change is approximately linear in the Nordic Seas. The maximum C_T change in this study amounts to 170 μmol kg^{-1} in the surface waters under the esmRCP8.5 scenario. The choice between pH or H^+ therefore has little impact on our results. The

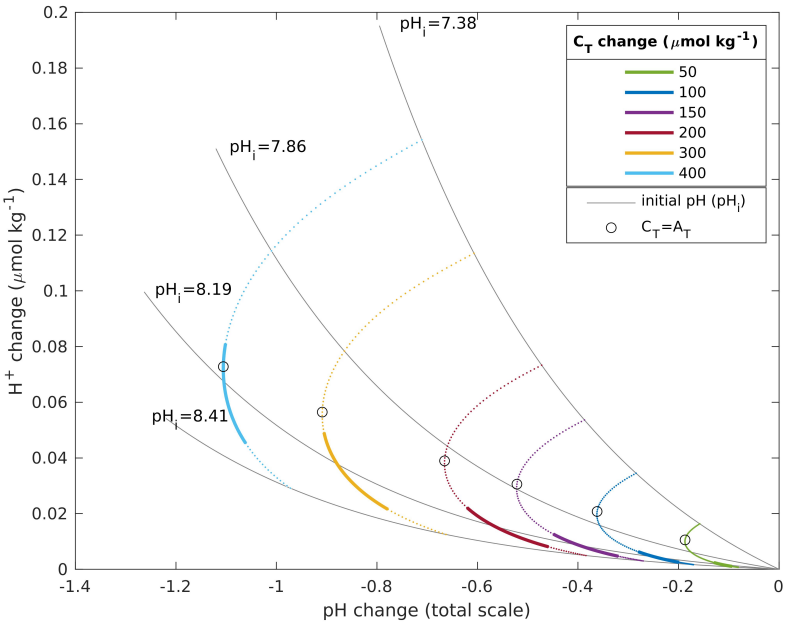

Figure 2. H^+ change plotted against pH change for six different increases in C_T (colored lines), for a range of initial pH. The upper and lower ends of the colored lines represents an initial pH of 7.38, and 8.41, respectively. The bold part of the lines represents the pH range in the Nordic Sea surface water in the GLODAPv2 climatology. The circles are plotted at the initial pH where the initial and final C_T over A_T ratio are centered around 1.

linear relationship breaks down, if pH decreases as a result of an increasing C_T over A_T ratio. The maximum pH change takes place at the buffer minimum, which is close to where C_T=A_T, approximately at (pK1+pK2)/2 (Frankignoulle, 1994; Fassbender et al., 2017; Middelburg et al., 2020), which in our example is at pH 7.6. The linear relationship between the H^+ and pH change does therefore not hold for pH ranges where relatively low initial pH values are included, as is the case for the examples in Fassbender et al. (2021), as well as for larger C_T changes. In these cases it is more appropriate to use H^+ for diagnosing ocean acidification.

4.4 Uncertainty analysis

There are several sources of uncertainties (σ) involved in our calculations of pH and Ω: measurement uncertainty (σ_{mes}), mapping uncertainty (σ_{map}) for the gridded product, and uncertainties related to dissociation constants (σ_{Kx}) used in the CO2SYS calculations. To estimate the total uncertainties in our calculations of pH and Ω, we used the error propagation routine in the MATLAB version of CO2SYS (Orr et al., 2018). The uncertainties in the input parameters (A_T, C_T, temperature, salinity, phosphate and silicate) were set to σ_{mes} for the single measurements, and $\sqrt{\sigma_{mes}^2 + \sigma_{map}^2}$ for the mapped product as well as for past and future estimates. As σ_{mes} and σ_{map}, the product consistency from Olsen et al. (2019), and the mapping error (3D

field) from Lauvset et al. (2016), were used, respectively. The correlation between uncertainties in A_T, C_T were set to 0. This is a reasonable assumption given that C_T and A_T are measured on different instruments using different analytical methodologies. In addition, including a positive correlation term would decrease the overall uncertainty and we prefer a potential overestimation. For the dissociation constants the default uncertainties in the errors.m function were used. From here on, the calculated uncertainties will be presented as σ_{point} for discrete data, when σ_{Kx} and σ_{mes} are included, and σ_{field} for 3D data, when σ_{Kx}, σ_{mes} and σ_{map} are included.

For the observations described in Section 3.1, the mean, maximum and minimum uncertainties (σ_{point}) for our calculations of pH, Ω_{Ar}, Ω_{Ca} and pCO_2 are listed in Table 2. Variations in the uncertainties arise from variations in temperature and salinity, which impact the uncertainty of dissociation constants. While systematic uncertainties would tend to cancel out when calculating trends (i.e.,comparing measurements from the same location but from different times), random uncertainties would not (Orr et al., 2018). Therefore, to estimate to what extent these uncertainties could impact our trend estimates, we further investigated whether there is any trend in the uncertainties. This is discussed in Sect. 5.4.

For the GLODAPv2 estimate of pre-industrial C_T there is an additional uncertainty coming from the TTD method that was used to calculate the anthropogenic CO_2. He et al. (2018) published a thorough analysis of the different sources of uncertainty in this method, and concluded that the overall uncertainty is 7.8-13.6%. Combining this with the mapping errors, Lauvset et al. (2020) estimate that the global ocean anthropogenic carbon inventory calculated from the mapped fields is 167$\pm$29 PgC. This results in an uncertainty of 0.02 in the pre-industrial Nordic Seas upper layer pH.

Table 2. Uncertainties (σ_{point}, mean, max and min) in pH, Ω_{Ar}, Ω_{Ca} and pCO_2 (μatm), calculated from the individual observations described in Section 3.1.

	mean	max	min
pH	0.017	0.022	0.014
Ω_{Ar}	0.085	0.174	0.037
Ω_{Ca}	0.134	0.271	0.058
pCO_2	14.387	53.608	5.901

In the trends of the uppermost layer (0-200 m), there is also an uncertainty related to seasonal undersampling. Most samples (about 60% in total) from the data sets described in Sect. 3.1 were collected during spring and summer (April-September, Figs. S8 -S13). The uneven sampling frequency of different seasons introduces uncertainty in the annual means of the uppermost ocean layer, and can lead to biases in our trend estimates. Unfortunately, there are not enough data to allow for de-seasonalization in order to remove such potential biases. Therefore, to get an idea of the effect of seasonal undersampling we additionally calculated trends by using annual means containing samples from the productive season only, both for a longer period (April-September) to include both the spring bloom and the summer production, and for a shorter period (June-August), to include only the summer season.

Modelled future projections are uncertain due to incomplete understanding or parameterization of fundamental processes, as well as different and unknown future carbon emission scenarios (Frölicher et al., 2016). Because this study primarily focuses

Table 3. Spatial correlation (r) and explained variance (r^2, in paranthesis) between pH and pH(T), pH(T,C_T,A_T) and pH(T,C_T,A_T, S), and between Ω_{Ar} and Ω_{Ar}(C_T,A_T), Ω_{Ar}(C_T,A_T, T) and Ω_{Ar}(C_T,A_T, T, S) in the Nordic Seas surface (0 m) waters. Numbers in bold indicate significant correlation.

Drivers	(T)	(T,C_T,A_T)	(T,C_T,A_T,S)
pH	**0.58** (0.34)	**0.94** (0.89)	**1.00** (1.00)
Ω_{Ar}	**0.85** (0.73)	**1.00** (1.00)	**1.00** (1.00)

on process understanding and the driving factors behind pH change, we do not consider model uncertainty in Sect. 5.3,5.5, and 5.7.2, where the drivers of pH changes in the model projections are analysed. However, in Sect. 5.6, where the future aragonite saturation horizon is presented, we do account for model uncertainty. The model dependent uncertainty, here defined as the model spread, of the future saturation horizon under the esmRCP8.5 scenario, was estimated by adding the modelled change in C_T and A_T for each model of our ESM-ensemble to the GLODAPv2 climatologies. Model differences in changes of temperature, salinity, phosphate and silicate are neglected because they are minor in comparison to the effect of the changes in C_T and A_T (This is further discussed in Sect. 5.7.2). Internal climate variability is an additional source of model uncertainty that we do not explicitly account for in this study. However, a large part of this variability is eliminated because we use 10 year means for the future and past estimates of pH.

5 Results and discussion

This Section is organized as follows: we will start to describe the present distribution of pH and Ω_{Ar} and its drivers (Section 5.1). In Section 5.2, we give an overview of pH changes from pre-industrial to 2100. Thereafter we describe regional changes from pre-industrial to present-day (Section 5.3), present-day changes (Section 5.4), changes from present-day to future (Section 5.5) and assess its impacts on cold-water corals (Section 5.6). In Section 5.7 we analyze the drivers of pH change in the different time periods.

5.1 Present-day spatial distribution of pH and Ω saturation states

Due to the contrasting properties of Atlantic waters, here defined as waters with salinity > 34.5, (Malmberg and Désert, 1999; Nondal et al., 2009) and polar waters (defined as the waters with salinity < 34.5 detached from the Norwegian coast) that meet and mix in the Nordic Seas, there are large spatial gradients in surface (0 m) temperature, salinity and chemical properties (Fig. 3 and S14). The Atlantic Water, located in the eastern part of the Nordic Seas, is characterized by higher temperature, salinity, and A_T, while polar waters are colder and fresher with lower A_T. This results in a decrease in temperature, salinity, and A_T from southeast to northwest. Within the Atlantic water there is a tendency of increasing C_T with decreasing temperature. This is largely as a consequence of the increased CO_2 solubility in colder water, i.e., a cooling of a water mass result in an increase in C_T due to an uptake of CO_2 from the atmosphere. In polar waters, C_T is lower than in Atlantic waters due to the lower

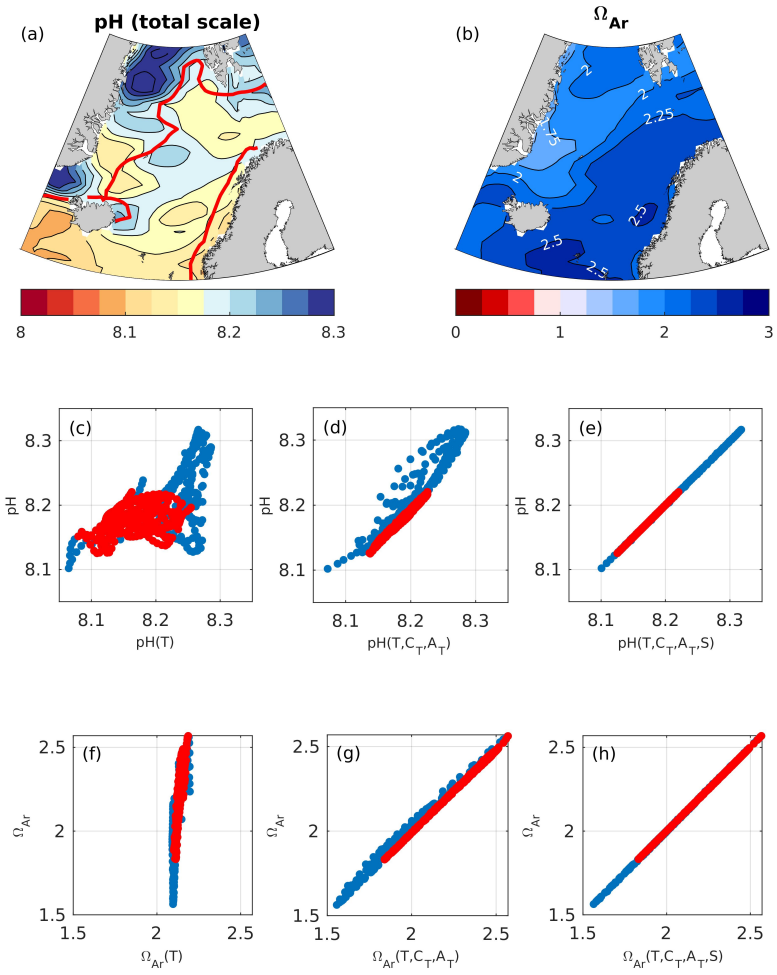

Figure 3. Maps of present-day surface (0 m) pH (a) and Ω_{Ar} (b). The solid red line in (a) mark the border between Atlantic Water (salinity>34.5) and low salinity waters (salinity<34.5). The low saline waters include Norwegian coastal waters (constrained to the Norwegian coast) and polar waters (constrained to the north-western part of the domain). pH and Ω_{Ar} plotted against variations induced by temperature (c,f), temperature and $C_T + A_T$ (d,g) and temperature, $C_T + A_T$ and salinity (e,h) in pH and Ω_{Ar}, calculated as described in Section 4.1 in Atlantic Water (red) and low salinity waters (blue). Each circle represents a value from a single grid cell.

pCO_2 (Fig. S14)), and also as a result of the large freshwater export from the Arctic Ocean that dilutes not only C_T, but also A_T and salinity.

The surface pH in the Nordic Seas increases from Atlantic waters to polar waters (Fig. 3). The correlation between the pH and the pH calculated with spatially varying temperature only (pH(T)), keeping all other drivers constant, is 0.58. This means that temperature-induced variations (through the thermodynamic effect) are able to explain 34% of the spatial variability in pH (Fig. 3 and Table 3). Adding C_T+A_T and salinity contributions explains an additional 55% and 11%, respectively, of the spatial variability in pH. The effect of salinity is largest in the low-salinity regions, i.e., in polar waters and the Norwegian coastal waters. In contrast to what is suggested by directly correlating pH and C_T+A_T (Table S9), the results in Table 3 show that C_T+A_T are important contributors to spatial variations in pH. This indicates that the influence of C_T and A_T on pH is masked out by temperature variations in Table S9 and Fig. S15, which can be explained by the two cancelling effects that temperature has on pH (Jiang et al., 2019). For example, while the instantaneous, thermodynamic effect of a drop in temperature leads to a pH increase, it also results in a drop in pCO_2, which subsequently leads to an anomalous CO_2 uptake from the atmosphere. This increases the C_T/A_T ratio, which in turn causes a drop in pH that counteracts the initial thermodynamic affect.

The saturation state Ω_{Ar} show an opposite pattern to pH, with low saturation states in polar waters, and high saturation states in Atlantic Water. From Fig. 3d, it becomes clear that the temperature effect on the solubility of Ω_{Ar} (Ω_{Ar}(T)) only explain 11% of the observed Ω_{Ar} range, although it is able to explain 98% of the variability. When adding C_T+ A_T contributions, the observed range in Ω_{Ar} is reproduced, and 100% of the variability is explained. C_T+A_T strongly influences Ω_{Ar}, because with decreasing C_T to A_T ratio, the CO_3^{2-} concentration decreases as well. The C_T to A_T ratio itself strongly correlates with temperature as the CO_2 solubility increases with decreasing temperature and vice versa (S9). The strong correlation between Ω_{Ar} and temperature (Table S9) is therefore largely a result of the temperature effect on C_T+A_T, and as such, the CO_3^{2-} concentration, (Sect. 2 and Orr (2011); Jiang et al. (2019)). Thermodynamic salinity induced variations only have a minor contribution to the spatial variations in Ω_{Ar} (less than 1%), and, as for pH, the effect of salinity is more prominent in the low salinity-regions.

5.2 Overview of modelled and observed pH changes from pre-industrial to the end of the 21st century

Here we give an overview of upper layer, taken to be the upper 200 m for both model and observations, pH changes in the Nordic Seas from 1850 to 2100 (Fig. 4). Note that in this section we use the actual modelled pH data, and not the modelled change applied to observational data, and use this as an opportunity to evaluate the model's performance. The pre-industrial average Nordic Seas surface pH estimated in GLODAPv2, using an atmospheric CO_2 of 280 ppm, and NorESM1-ME, using year 1850 with an atmospheric CO_2 of 284 ppm, are in good agreement, with mean values of 8.21$\pm$0.02 and 8.22$\pm$0.02, respectively. From 1850 to 1980, the emission-driven NorESM1-ME simulates an average pH decline of 0.06 in the Nordic Seas, while the concentration-driven run simulates a drop of 0.05 (Fig S5). The difference is caused by the slight deviation in atmospheric CO_2 between emission-driven historical run and historical data (See Sect. 3.3).

For the period between 1981 and 2019, the modelled pH largely encompasses the observed one (within the spatial standard deviations), showing that the pH of the Nordic Seas surface water is reasonably well simulated. The pH trend estimated from the observations for this period, -2.64$\pm$0.31 10^{-3} yr^{-1}, is not significantly different (at the 95% confidence level) from the modelled pH trend, -2.21$\pm$0.04 10^{-3} yr^{-1}. Because the pH calculated from observational data is based on discrete samples

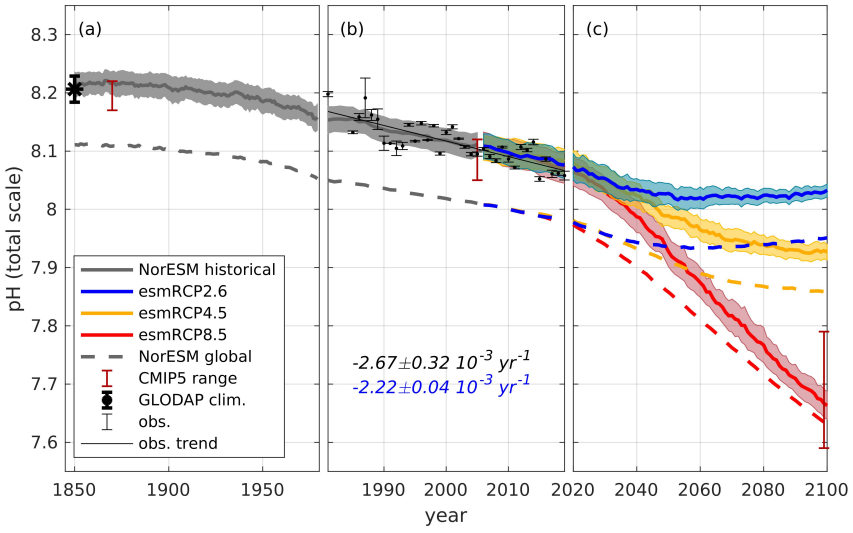

Figure 4. pH evolution, averaged over the Nordic Seas surface waters (0-200 m), from 1850 to 2100, separated into a) past (1850-1980), b) present-day (1981-2019) and c) future (2020-2100). Black dots with error bars show the observed annual mean pH, with standard deviations (due to spatial/seasonal variations), determined from all available observations in the Nordic Seas as shown in Fig. 1. The solid black line shows the trend calculated from these observations. The gray, red, yellow and blue solid lines show NorESM1-ME output for emission-driven historical and future (esmRCP8.5, esmRCP4.5 and esmRCP2.6) simulations, respectively, where the shading depicts the spatial variation (standard deviation). Note that the atmospheric CO_2 increase as simulated by NorESM1-ME for 1850 to 2005 deviates by 14 ppm from the actual measured increase, which results in a simulated pH decrease that is 0.01 stronger than expected (See Sect. 3.3). The red vertical bars display the pH range in the CMIP5 model ensemble for the historical and esmRCP8.5 simulations. The figure illustrates the actual modelled pH data, and not the modelled change applied to observational data. The dashed lines show the evolution of global surface ocean pH from the same simulations. The black asterisk (1850) with error bars show an estimate of the pre-industrial mean pH with spatial standard deviation, derived from the GLODAPv2 mapped product as described in Sect. 3.2. The numbers in black and blue show the calculated and significant linear trend with standard errors from the observations and the model, respectively, for the period of 1981-2019.

with a limited spatial and temporal coverage, its representativeness for the entire Nordic Seas is questionable, and we do not expect an exact agreement with the model. For example, the stronger trend obtained from the observational data might be a result of the samples in the beginning of the period being biased to regions with higher pH.

The future evolution of upper layer pH in the Nordic Seas depends strongly on the CO_2 emission scenario (Fig. 4). In the esmRCP2.6 scenario, where the CO_2 emissions are kept within what is needed to limit global warming to 2 °C (van Vuuren et al., 2011b), pH drops by 0.04 from 2020 to 2099, and reaches a value of 8.03±0.01. Note that in this scenario there is a peak and decline, related to the overshoot profile of the atmospheric CO_2 concentration, with a minimum pH value in mid-century. For the esmRCP4.5 scenario, which corresponds roughly to the currently pledged CO_2 emission reductions under the Paris agreement, the surface pH is simulated to drop by about 0.15, reaching an average value of 7.93±0.01 by the end of the 21st

century. Under the high-CO_2 esmRCP8.5 scenario, NorESM1-ME simulates the pH to decrease by 0.40 between 2020 and 2099 to an average value of 7.67±0.02. This equals a pH decline of approximately to -5.00 10^{-3} yr^{-1}. The model related uncertainty in the esmRCP8.5 scenario, measured as the inter-model spread of pH in 2099, displays a pH range of 7.59-7.79 in the surface layer (Fig. 4, S5). This spread is larger than that observed in the concentration-driven simulations with the same models, 7.69-7.75, as expected from the increased degrees of freedom brought about by the interactive atmospheric CO_2. Within the emission-driven model ensemble, the pH-decline from pre-industrial to the end of the 21st century as simulated by NorESM1-ME is among the strongest, which most likely is a result of a simulated stronger increase in atmospheric CO_2. A full analysis of the reasons behind the inter-model spread is beyond the scope of this paper.

The simulated Nordic Seas average upper layer pH is 0.11 higher than the global average in 1850, which is related to the undersaturation of CO_2 in the surface waters of the Nordic Seas (Jiang et al., 2019). Our global average pH is about 0.1 lower than that estimated by, e.g., Jiang et al. (2019) for the surface ocean due to our consideration of a 200 m thick upper layer. The difference between the simulated upper layer pH of the global ocean and the Nordic Seas is decreasing with time. By the end of the 21st century, the Nordic Seas upper layer pH is 0.03, 0.07 and 0.08 higher than the global average for the esmRCP8.5, esmRCP4.5 and esmRCP2.6 scenarios, respectively. This is partially a result of the colder waters of the Nordic Seas, which gives them a lower buffer capacity. Additionally, in esmRCP8.5, there is an increase in the pCO_2 undersaturation of the global ocean that increases the global average pH (Fig. S16). Other factors driving this decreasing pH difference between the global ocean and the Nordic Seas can be differential heating. A quantitative assessment of the drivers is beyond the scope of this paper.

5.3 Modelled pH and Ω_{Ar} changes from pre-industrial to present-day

In this Section and the following, we present temporal changes in pH and Ω_{Ar}. Note that results for the modelled changes are referring to the 0 m surface, unlike the 0-200 m depth range that we use for the upper layer in Sect. 5.2 and 5.4.

From pre-industrial to present, the spatial pattern of changes in surface pH and Ω_{Ar} are similar (Fig. 5). The strongest decreases, reaching -0.12 and -0.55, respectively, are found in Atlantic Water along the Norwegian coast both for pH and Ω_{Ar}. The smallest change is found in polar waters (see more in depth discussion in Sect. 5.7.2). The corresponding maps for H^+ (Fig. S17) show a similar spatial distribution as for pH. Due to the longer ventilation time scales of deeper waters, the pH decrease weakens with depth. As shown in the section across 70°N (Fig. 6), waters below 2500 m are nearly unaffected. While the entire water column remains saturated with respect to calcite, the saturation horizon (Ω=1) of aragonite shoaled from a mean depth of 2200 m (uncertainty range: 2100-2400 m) during pre-industrial, to a present-day mean depth of 2000 m (uncertainty range: 1700-2300 m), across this specific section. Note that these depths were obtained from the contour interpolation when creating Fig. 6, which has a finer vertical resolution than the GLODAPv2 climatology.

5.4 Observed present-day changes in pH and Ω_{Ar}

Regional trends in observed seawater pH between 1981 and 2019 for five different depth intervals are presented in Fig. 7 and Table 4. The corresponding trends in H^+ are shown in Fig. S18 and Table S10. In the upper layer (0-200 m), significant trends

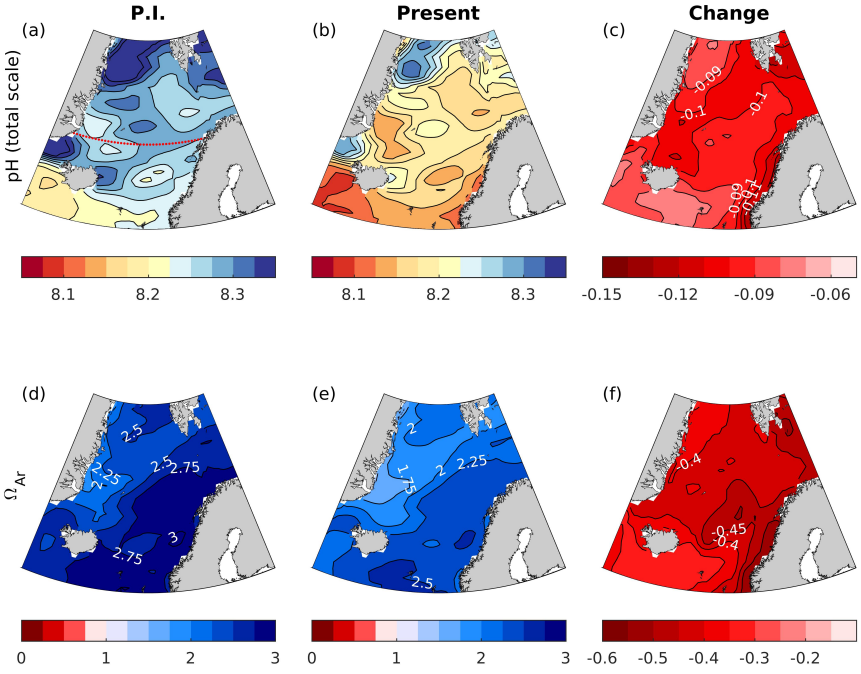

Figure 5. Maps of surface water (0 m) pH and Ω_{Ar} for pre-industrial (P.I., 1850-1859), present-day (1996-2005), and the change in between the two periods. The maps were calculated from the GLODAPv2 gridded climatologies (Lauvset et al., 2016) applying the simulated changes by the emission-driven NorESM1-ME, as explained in Sect. 4.2. Note that the increase in atmospheric CO_2 in NorESM-ME is 13% higher than the observed record between 1850 and 2005, resulting in an approximately 0.01 too strong decrease in surface pH (See Sect. 3.3). The dotted red line in (a) show the location of the cross-section presented in Fig. 6

.

Table 4. pH trends $\pm$ standard error (10^{-3} yr^{-1}) calculated from the data presented in Fig. 7, in the Norwegian Basin (NB), Lofoten Basin (LB), Barents Sea Opening (BSO), Fram Strait (FS), Greenland Sea (GS), and Iceland Sea (IS) (Fig. 1). Bold numbers indicate that the trends are significantly different from zero.

Depth (m)	NB	LB	BSO	FS	GS	IS
0-200	**-3.04±0.32**	**-2.40±0.23**	-1.67±0.77	**-2.53±0.74**	**-2.19±0.37**	**-3.10±0.30**
200-500	**-2.22±0.32**	**-1.89±0.31**	-1.05±0.82	**-1.49±0.42**	**-1.61±0.22**	**-2.51±0.27**
500-1000	**-1.17±0.27**	**-2.27±0.46**		-1.09±0.52	**-1.52±0.18**	**-1.84±0.29**
1000-2000	**-0.65±0.22**	-0.80±0.40		-0.55±0.81	**-1.36±0.15**	**-1.3±0.21**
2000-4000	0.46±0.55	-0.22±0.51		-0.03±0.69	-0.31±0.23	

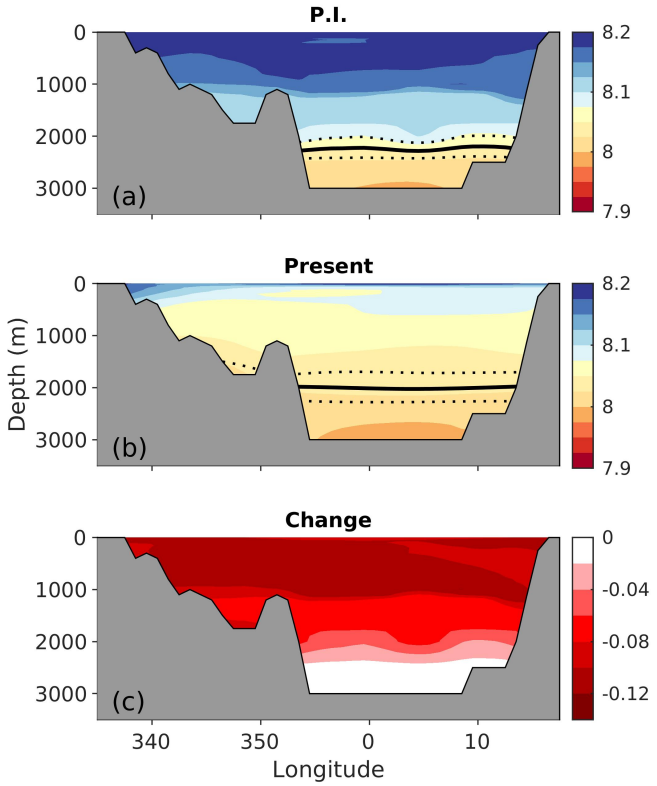

Figure 6. Zonal cross sections (at 70 °N) of pre-industrial (1850-1859) and present (1996-2005) pH, and the change between the two periods. Note that the simulated increase in atmospheric CO_2 of NorESM-ME is 13% higher than the observed record between 1850 and 2005, resulting in a simulated decrease in surface pH that is approximately 0.01 too strong (See Sect. 3.3). The solid black line shows the saturation horizon of aragonite (Ω_{Ar}=1). The dashed lines shows the associated uncertainties(σ_{field}).

Table 5. Ω_{Ar} trends $\pm$ standard error (10^{-3} yr^{-1}) calculated from the data presented in Fig. 8, in the Norwegian Basin (NB), Lofoten Basin (LB), Barents Sea Opening (BSO), Fram Strait (FS), Greenland Sea (GS), and Iceland Sea (IS) (Fig. 1). Bold numbers indicate that the trends are significantly different from zero.

Depth (m)	NB	LB	BSO	FS	GS	IS
0-200	**-11.97±3.25**	**-8.45±1.18**	**-8.29±3.54**	**-11.61±3.13**	-4.05±3.21	**-11.20±2.22**
200-500	**-5.57±2.51**	-1.76±2.17	3.94±3.01	-2.06±1.60	**-3.19±0.61**	**-6.37±0.74**
500-1000	**-4.28±1.25**	-5.55±3.38		-1.11±1.46	**-2.98±0.52**	**-4.52±0.71**
1000-2000	**-3.49±1.24**	0.03±1.76		0.65±3.08	**-2.98±0.59**	**-2.57±0.50**
2000-4000	3.67±1.82	0.33±1.57		1.13±1.53	0.53±0.80	

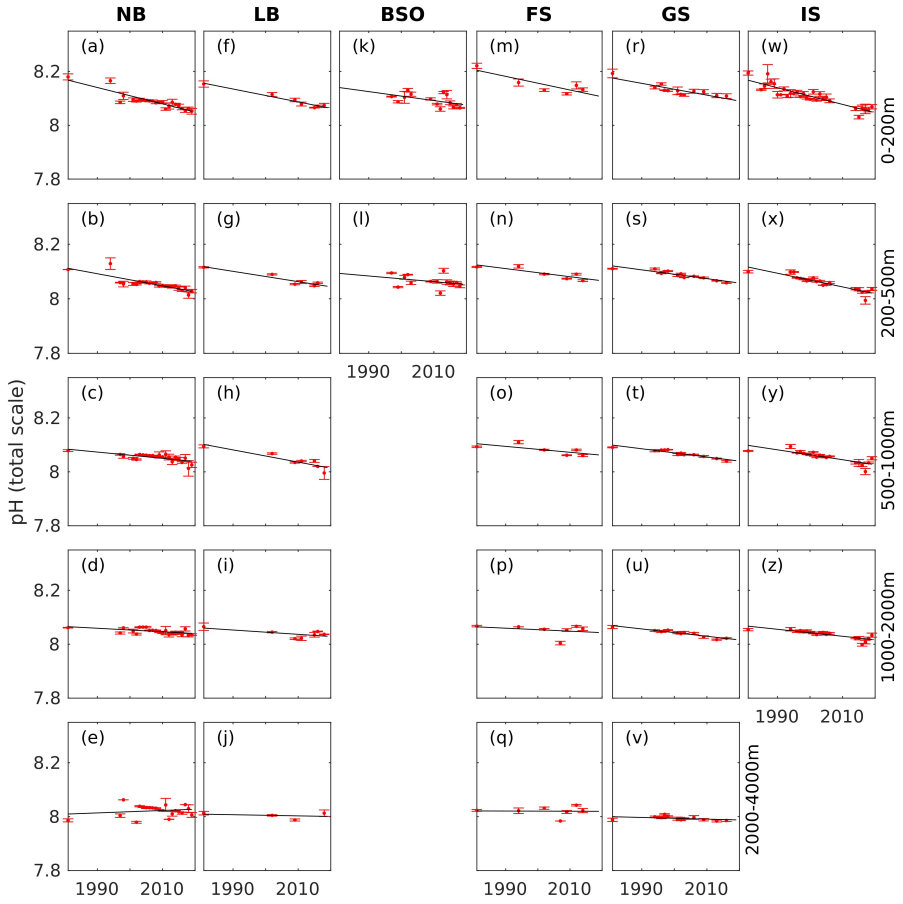

Figure 7. Annual mean pH (red dots) with standard deviation (error bars) at five different depth intervals in the Norwegian Basin (NB), Lofoten Basin (LB), Barents Sea Opening (BSO), Fram Strait (FS), Greenland Sea (GS), and Iceland Sea (IS) (Fig. 1), calculated as described in Sect. 4.2. The solid black line show the trend estimate from the linear regression.

of 2-3 10^{-3} yr^{-1} are found in all basins except for the Barents Sea Opening. The uncertainties (standard errors) of these trends are between ± 0.2 and ± 0.8 10^{-3} yr^{-1}. Due to the difference in sampled years, we cannot robustly compare the magnitude of trends between the basins. Skjelvan et al. (2014) also found significant trends in upper 200 m pH of the Norwegian and Lofoten basins and of the Greenland Sea for the period of 1981-2013. Our estimated trend in the Norwegian Basin of -3.04 $\pm$ 0.32 10^{-3} yr^{-1} is weaker than their -4.1 10^{-3} yr^{-1} trend, which can be a result of different sampling period and slightly different definition of regions. However, our trend estimates in the Greenland Sea and Lofoten Basin of -2.19 $\pm$ 0.37 10^{-3} yr^{-1} and -2.40 $\pm$ 0.23 10^{-3} yr^{-1}, respectively, agrees well with the trend of -2.3 10^{-3} yr^{-1} that they calculated for both regions. The non-significant trend we find in the Barents Sea Opening is also in agreement with the results of Skjelvan et al. (2014). In contrast to their results, we obtained a significant trend in the eastern Fram Strait, which may be a result of the larger time span of our dataset. As expected from the generally longer ventilation time scales of deep waters, the trends in pH decline with

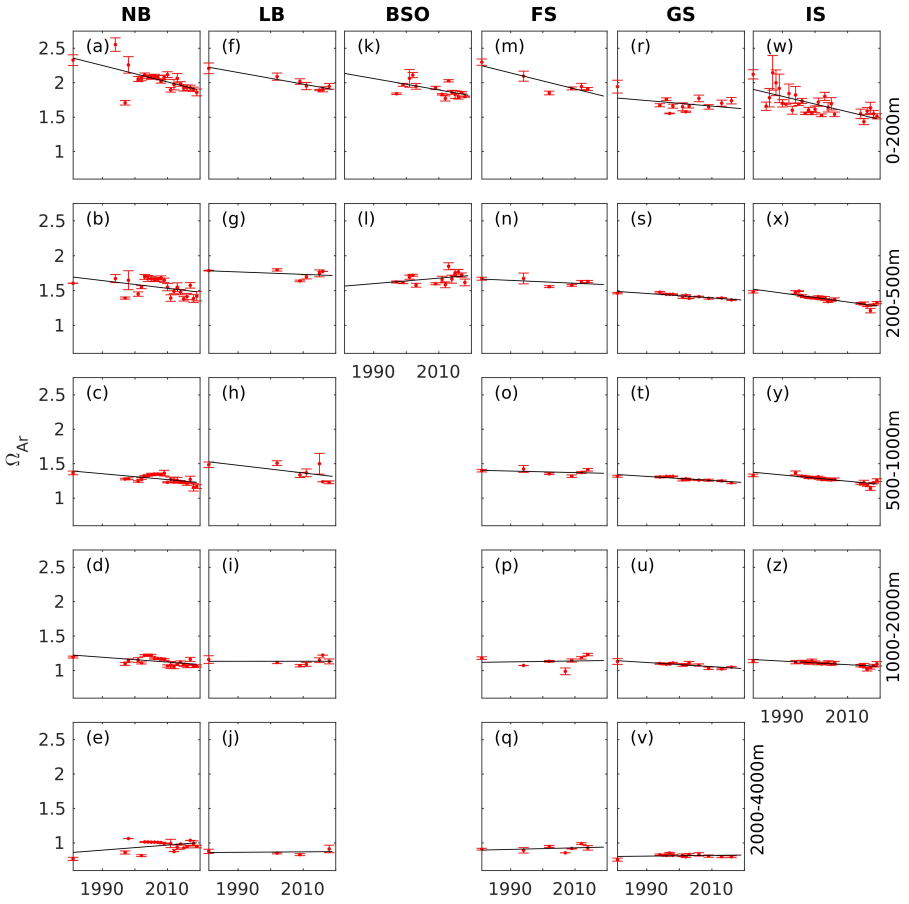

Figure 8. Annual mean Ω_{Ar} (red dots) with standard deviation (error bars), at five different depth intervals, in the Norwegian Basin (NB), Lofoten Basin (LB), Barents Sea Opening (BSO), Fram Strait (FS), Greenland Sea (GS), and Iceland Sea (IS) (Fig. 1), calculated as described in Sect. 4.2. The solid black line show the trend estimate from the linear regression.

depth. Significant trends are detected down to 2000 m in the Greenland Sea, in agreement with Skjelvan et al. (2014), but also in the Iceland Sea and in the Norwegian Basin. In the Lofoten Basin and eastern Fram Strait, the decrease in pH is significant down to the 1000 m and 500 m layers, respectively. As for the upper layer, no significant trend is found in the 200-500 m layer in the shallow Barents Sea Opening.

Trends of aragonite saturation states are shown in Fig. 8 and Table 5. As for pH, the rate of change is strongest in the upper layer. For Ω_{Ar}, the decline is in the order of 10^{-2} yr^{-1} and significant in all regions except for the Greenland Sea. The weak decline in the Greenland Sea surface layer is a result of a smaller increase in C_T in combination with relatively strong increases in A_T and temperature, which counteracts the effect of C_T on the saturation states (while the temperature amplifies pH declines, see Sect. 2). The reduction in Ω_{Ar} is significant down to 2000 m in the Norwegian Basin and the Greenland and Iceland Seas. In the other regions, no significant decline has occurred below the surface layer. In the depth layers considered,

aragonite undersaturation occurs in the 2000-4000 m layer. The waters in the depth range 1000-2000 m are close to the limit of undersaturation. The smallest values in this layer are 1.05, 1.07, 0.99, 1.02, and 1.01, for the Norwegian Basin, Lofoten Basin, eastern Fram Strait, Greenland Sea and Iceland Sea, respectively. Considering the associated uncertainties of 0.06 (Table 2), this is indistinguishable from undersaturation in all regions except for the Lofoten Basin. In contrast to Skjelvan et al. (2014) who only found a significant negative trend in the upper 200 m layer of the Norwegian Basin, we are now, with the longer time series, able to state that there is a significant decrease in Ω_{Ar} in several regions and at several depth layers.

During the period 1981-2019, we detect trends in the uncertainties of pH and Ω_{Ar} (Figs. S6 and S7), reaching -0.04 10^{-3} yr^{-1} and 0.53 10^{-3} yr^{-1}, respectively. These are, however, about two orders of magnitude smaller than the trends in pH and Ω_{Ar}, and they do therefore not significantly impact interpretation of our results.

5.5 Modelled pH and Ω_{Ar} changes from present-day to future

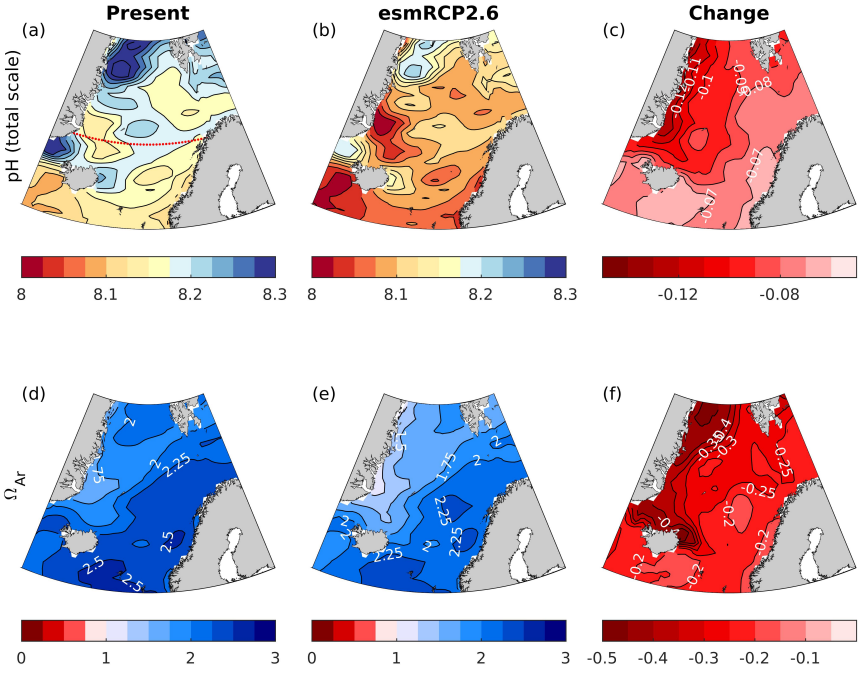

Figure 9. Maps of surface water (0 m) pH and Ω_{Ar} for the present-day (1996-2005) and the esmRCP2.6 future (2090-2099), as well as the changes between the periods. The data-input of the maps is based on GLODAPv2 gridded climatologies combined with the change from the NorESM1-ME. The dotted red line in (a) show the location of the crossection presented in Fig. 10.

In this section we go into regional details of future pH and Ω_{Ar} changes under the esmRCP2.6 and the esmRCP8.5 scenarios. The results are presented for the surface (0 m), and not for the upper layer 0-200 m as in Sect. 5.2 and 5.4.

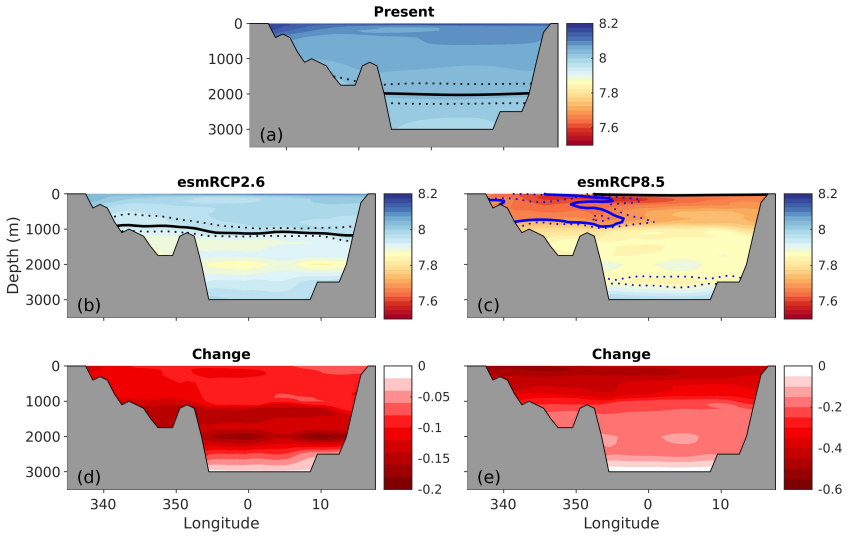

Figure 10. Zonal cross sections (at 70 °N) of present (1996-2005) and future (2090-2099) pH under the emission-driven esmRCP2.6 and esmRCP8.5 scenarios, along with the change between the periods. The solid and dotted black lines show the saturation horizon of aragonite (Ω_{Ar}=1) with uncertainty (σ_{field}). The solid and dotted blue line show the corresponding for calcite (Ω_{Ca}=1).

In esmRCP2.6, a pH decline of 0.06-0.11 in the surface waters is simulated between present-day (1996-2005) and future (2090-2099) (Fig. 9c). The largest pH decreases are found in polar waters, leading to a weakening of the present-day zonal pH gradient. Surface Ω_{Ar} is projected to decrease by about 0.2-0.5 under esmRCP2.6, with the largest drops taking place in polar waters. Surface waters remain supersaturated with respect to both calcite and aragonite. Interestingly, the strongest ocean acidification occurs at depths of 1000-2000 m in this scenario (Fig. 10c), which leads to a shoaling of the aragonite saturation horizon to a depth of 1100 m (uncertainty range: 800-1200 m). This is discussed in more detail in Sect. 5.7.2.

Under the esmRCP8.5 scenario, surface pH drops by about 0.4-0.5 between present-day and future (Fig. 11), with the largest decreases in polar waters. Surface Ω_{Ar} drops by around 1.1-1.3. In contrast to esmRCP2.6, the largest decline of Ω_{Ar} take place in the Atlantic Water. The reason behind this is discussed in Sect. 5.7.2. The strong ocean acidification in this scenario leads to a reversal of the pH depth-dependency so that pH increases from surface to depth by the end of the 21st century (Fig. 10c). Here, the anthropogenic carbon input at the surface overrides the effect of pressure and organic matter remineralization on the vertical pH gradient. The change in Ω_{Ar} is large enough to bring the entire water column, and consequently also the entire seafloor, to aragonite undersaturation. The only exception is a thin surface layer (above 30 $\pm$10 m) in the Atlantic Water region. For all emission scenarios the spatial distribution of H^+ and its change (shown in Fig. S19 and Fig. S20) are similar to that of pH.

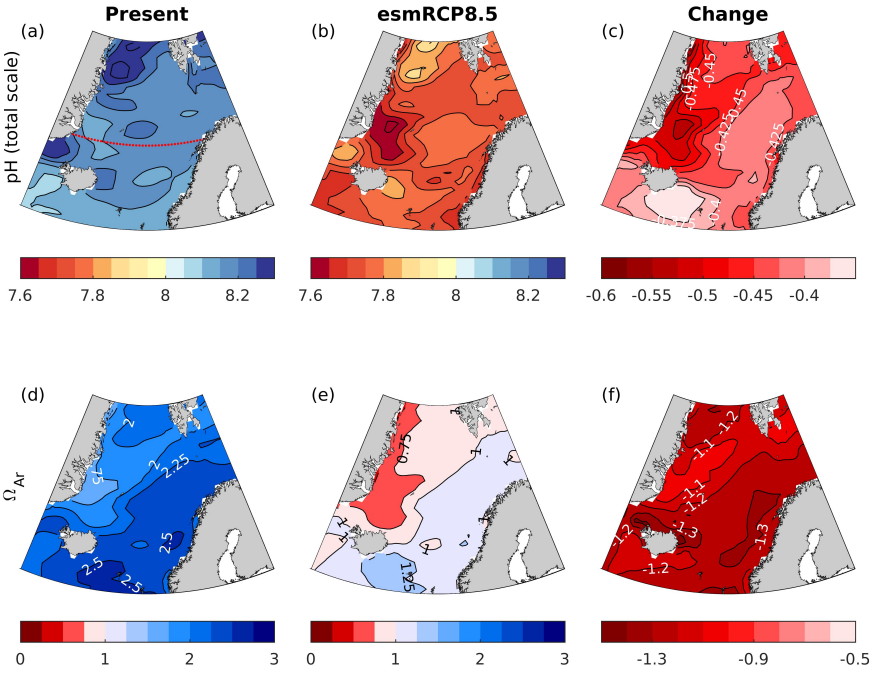

Figure 11. Maps of surface water (0 m) pH and Ω_{Ar} for the present (1996-2005) and the esmRCP8.5 future (2090-2099), as well as the changes between the periods. The data-input of the maps is based on GLODAPv2 gridded climatologies combined with the change from the NorESM1-ME. The dotted red line in (a) show the location of the crossection presented in Fig. 10.

5.6 Implications for cold-water corals

Cold-water corals build their structures out of aragonite, which is the more soluble form of calcium carbonate. These corals can, to some degree, compensate for aragonite undersaturation in seawater by increasing their internal pH by 0.3-0.6 (McCulloch et al., 2012; Allison et al., 2014). For some time, they can therefore continue to calcify in waters with Ω_{Ar}<1. However, the calcification rates and breaking strength of the structures of the most abundant coral organism, *Lophelia pertusa*, is reduced under such conditions (Hennige et al., 2015). Furthermore, dead coral structures, which compose the major part of the reefs, cannot resist corrosive waters and experience increased dissolution rates at Ω_{Ar}<1. Cold-water coral reefs, along with their ecosystems, are consequently likely to collapse if the water they live in becomes undersaturated with respect to aragonite. It has been estimated that about 70% of the deep sea corals globally will be below the aragonite saturation horizon by the end-of-the-century under high-emission-scenarios (Guinotte et al., 2006; Zheng and Cao, 2014).

Most of the reef sites that have been identified in the Nordic Seas (321 out of the 324 within the region defined in Fig. 1) are at depths of 0-500 m (Fig. 12, see also Buhl-Mortensen et al. (2015)). The aragonite saturation horizon estimated from the GLODAPv2 climatology for present climate is at 2000 m, with uncertainty range 1750-2500 m. Note that the uncertainty

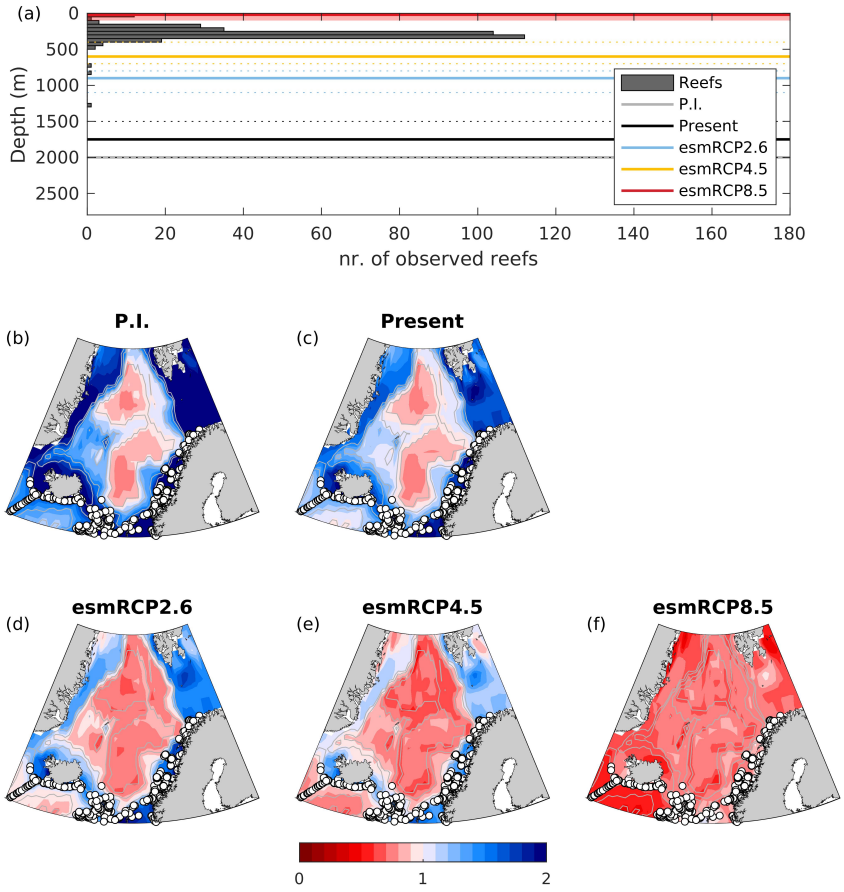

Figure 12. Number of observed reef sites per 50 m depth interval together with the aragonite saturation horizons (solid lines) in the Nordic Seas for past (1850-1879), present-day (1980-2005) and future (2070-2099) under the esmRCP2.6, esmRCP4.5 and esmRCP8.5 scenarios calculated from the GLODAPv2 climatology and NorESM1-ME simulations. The dashed lines show the uncertainty (σ_{field}). The red shading shows the projection uncertainty as estimated from our ESM ensemble for esmRCP8.5. (a) and maps showing aragonite saturation state of bottom waters (calculated from the GLODAPv2 climatology and NorESM1-ME simulations) together with positions of observed reefs (b-f).

range of the depth of the saturation horizon is not equally distributed around the mean because the uncertainty analysis is done for the saturation state, from which the depth distribution is calculated. From the discrete measurements we also see that the waters in the depth range 1000-2000 m are close to being undersaturated with respect to aragonite (Sect. 5.4). For the time being, the saturation horizon is thus well below the majority of the cold-water corals in the Nordic Seas.

505 In the esmRCP2.6 scenario, NorESM1-ME projects that the aragonite saturation horizon will shoal to 900 m (uncertainty: 800-1100 m), while in the esmRCP4.5 scenario the saturation horizon is projected to shoal to 600 m depth (uncertainty: 400-700 m) by the end of this century. This implies that the deepest observed reefs will be exposed to corrosive waters, and thus

experience elevated costs of calcification and dissolution of dead structures. The majority (315 out of 324) of the coral sites in the Nordic Seas are, however, found at shallower depths than the projected saturation horizon with uncertainty, although the margins are small. Also García-Ibáñez et al. (2021) suggested that cold-water corals in the subpolar North Atlantic will be exposed to corrosive waters if the 2 °C goal (which is the aim of RCP2.6) is not met. In the esmRCP8.5 scenario, NorESM1-ME projects the whole water column below 20 m (uncertainty: 10-20 m) to be undersaturated with respect to aragonite at the end of this century, such that all cold-water coral reefs in the Nordic Seas will be exposed to corrosive waters. For esmRCP8.5 the NorESM1-ME results are consistent with our CMIP5 model ensemble that suggests the future saturation horizon lies in the range of 0 and 100 m. Comparison with the CMIP5 ensemble is not possible for esmRCP2.6 and esmRCP4.5 because few of the models have performed emission-driven runs under these scenarios. However, NorESM1-ME simulates one of the stronger pH-declines in all depth layers considered in Fig. S5 (Table S6), and has also been shown to be on the upper end of absorption of anthropogenic carbon in the Arctic Ocean (Terhaar et al., 2020a), suggesting that our estimates of the future saturation horizon lies in the shallower end of possible future states.

5.7 Drivers of Ocean Acidification

5.7.1 Present-day drivers

To understand what has caused the observed pH changes presented in Sect. 5.4, we decompose the trends into their different drivers as described in Sect. 4.2 (Fig. 13). In the upper layer (i.e., 0-200 m) the pH decrease in the period 1981-2019 is in agreement (within 95% confidence) with the pH change expected from the increase in atmospheric CO_2, except for in the Norwegian Basin and the Iceland Sea where the trends are stronger. This is related to a faster increase in the seawater pCO_2 compared with that of the atmosphere (Fig. S21), meaning that the pCO_2 undersaturation of the Norwegian Basin and the Iceland Sea is has decreased. We note that this diminishing undersaturation is sensitive to seasons. In the Norwegian basin there is no significant decrease if using data from only April to September and June to August, respectively. In the Iceland Sea the decreasing undersaturation is absent for April-September, but it becomes stronger than the annual mean if using data only from June-August. The sensitivity to the choice of seasons indicates that the strong positive trend in the air-sea pCO_2 difference as seen in our dataset can be a result of seasonal undersampling, and that this should be verified with a larger dataset. Notwithstanding, diminishing pCO_2 undersaturation has been observed in earlier studies of the North Atlantic (Lefèvre et al., 2004; Olsen et al., 2006; Ólafsson et al., 2009; Metzl et al., 2010; Skjelvan et al., 2014), and could be a result of a change in any of the mechanisms underlying the pCO_2 undersaturation in surface waters of the Nordic Seas (see Sect. 1), including cooling of northward flowing Atlantic waters, primary production and the outflow of pCO_2 undersaturated waters from the Arctic Ocean. One other possible mechanism was suggested in Olsen et al. (2006) and Anderson and Olsen (2002), where they associated the fast increase in seawater pCO_2 with a large advective supply of anthropogenic carbon from the south and corresponding changes in the buffer capacity (see also Terhaar et al. (2020b)).

The main driver of the present-day (1981-2019) pH decrease in the upper layer is increasing C_T, which primarily is caused by biogeochemical processes ($C_T$bg), including increasing anthropogenic carbon, along with a small freshwater contribution

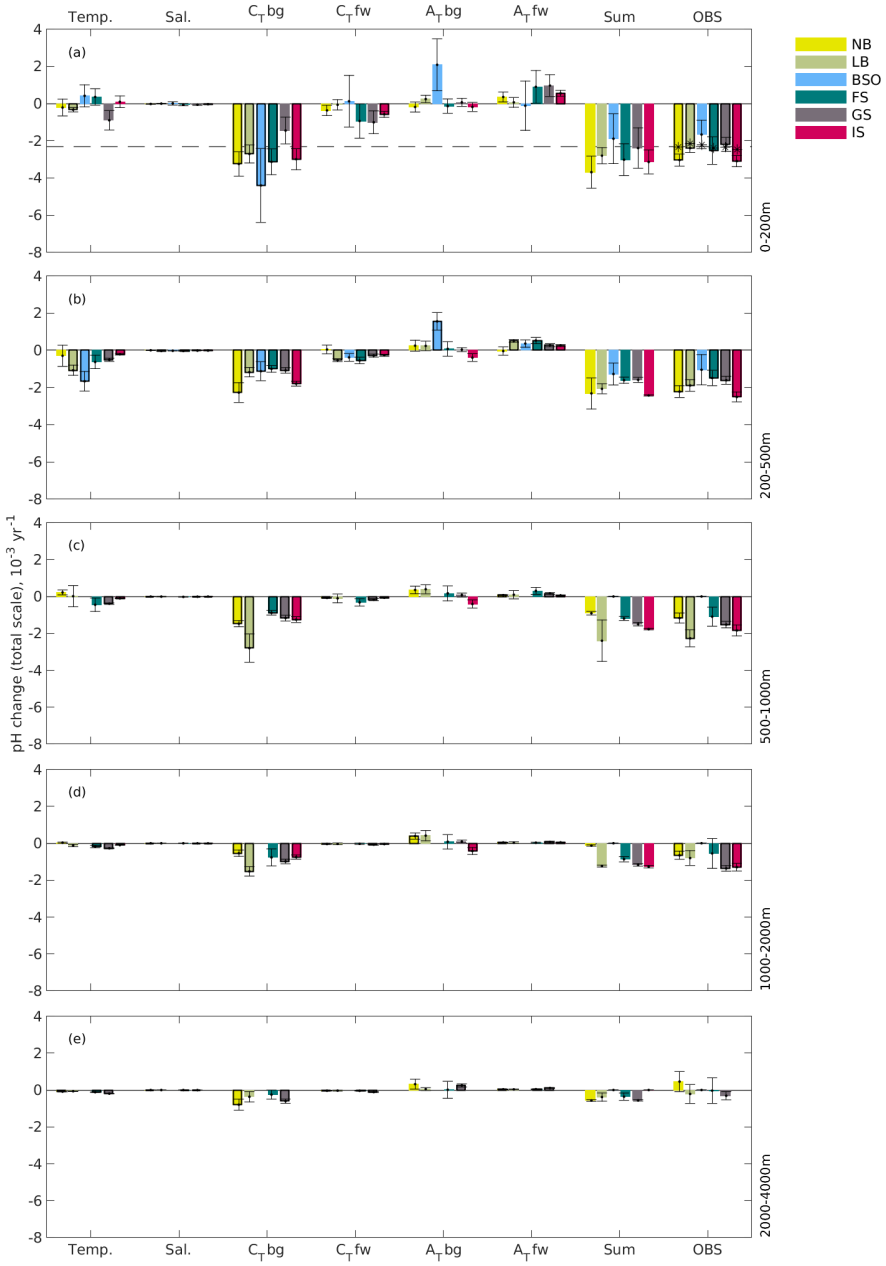

Figure 13. Contribution of observed changes in temperature, salinity, C_T, A_T to the observed trend in pH (OBS) over the 1981-2019 period, in the Norwegian Basin (NB), Lofoten Basin (LB), Barents Sea Opening (BSO), Fram Strait (FS), Greenland Sea (GS), and Iceland Sea (IS) (Fig. 1). The contribution of C_T, A_T was divided into a freshwater (fw) component and a biogeochemical (bg) component. Bars showing trends that are significantly different from zero are outlined with a black line. 'Sum' indicates the total trend in pH calculated as the sum of the trends associated with these six driving factors. The dashed line and black asterisks indicate the pH trends expected from the change in atmospheric CO_2 during the same period for the whole area and for the separate basins, respectively.

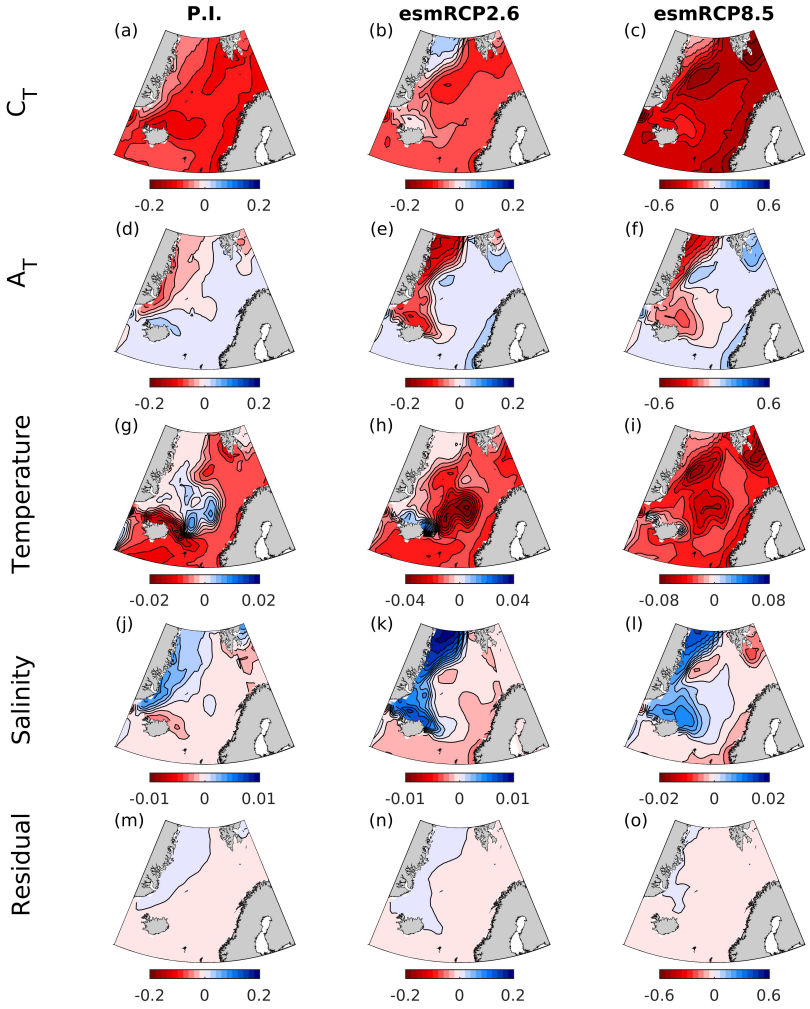

Figure 14. Contribution of modelled changes in surface C_T, A_T, temperature, and salinity, to the change in pH between 1850-1859 and 1996-2005 (P.I.), and 1996-2005 and 2090-2099 (esmRCP2.6 and esmRCP8.5). 'Res.' shows the residual between the total change in pH, calculated as the sum of the trends associated with these four driving factors, and the actual change shown in Figs. 5,9,11.

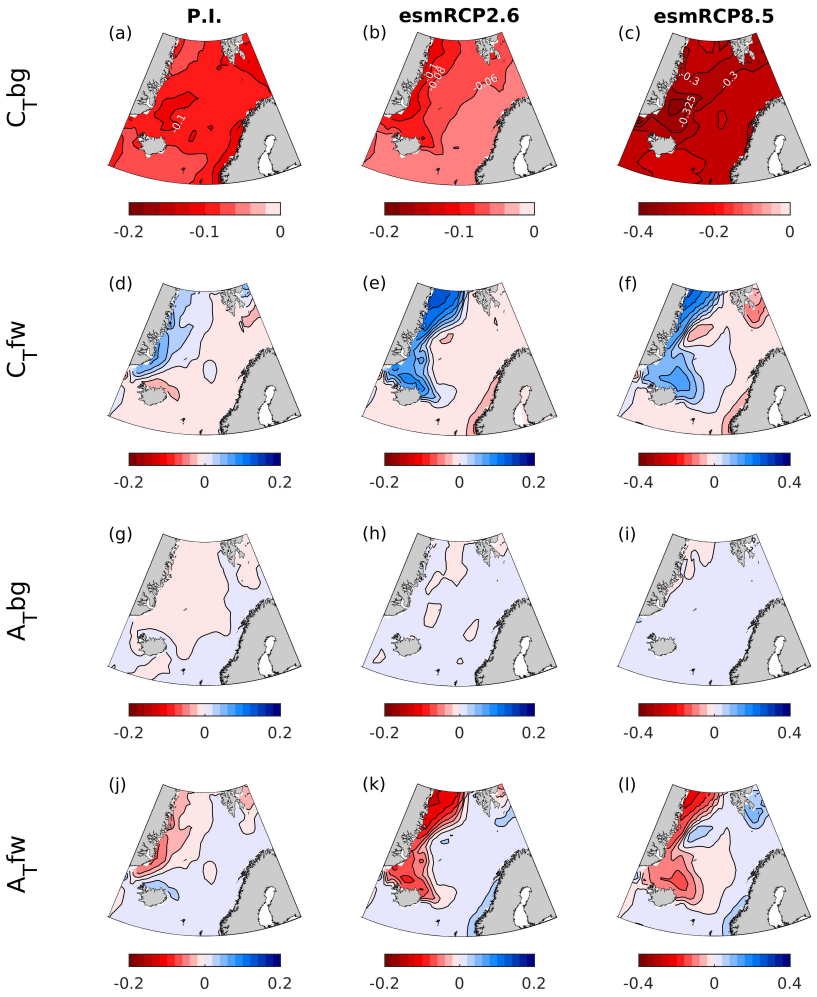

Figure 15. Contribution of the biogeochemical and freshwater components of C_T and of A_T ($A_T$bg and $A_T$fw) to the change in pH between 1850-1859 and 1996-2005 (P.I.), and 1996-2005 and 2090-2099 (esmRCP2.6 and esmRCP8.5). Residual shows the residual between the total change in C_T and A_T, calculated as the sum of the freshwater and biogeochemical components, and the actual change shown in Fig. 15

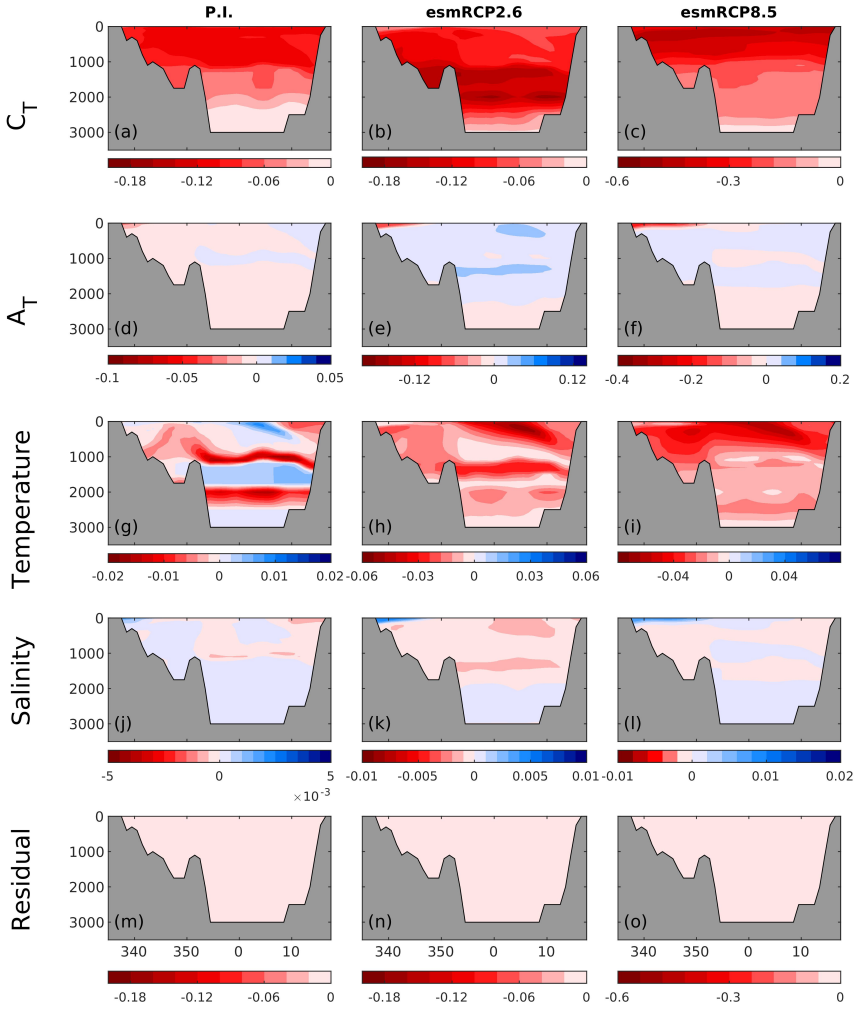

Figure 16. Contribution of modelled changes in surface temperature, salinity, C_T, A_T to the change in pH between 1850-1859 and 1996-2005 (P.I.), and 1996-2005 and 2090-2099 (esmRCP2.6 and esmRCP8.5) at the depth section at 70°N shown in Figs. 6,10. Residual shows the residual between the total change in pH, calculated as the sum of the trends associated with these four driving factors, and the actual change shown in Figs. 6,10.

($C_T$fw) caused by an increasing salinity (Fig. S2). The increasing salinity also results in an increasing A_T (Fig. S4). As seen in Fig. 13, the freshwater components of C_T and A_T are of equal size but opposite sign, and there is therefore no net effect of freshwater fluxes on the pH change (see Sarmiento and Gruber (2006) for a theoretical explanation). Also the thermodynamic effect of increasing salinity on pH is negligible. This increasing salinity of the Nordic Seas is a result of changes in the inflowing Atlantic Water related to subpolar gyre strength (Holliday et al., 2008; Lauvset et al., 2018). The contribution of the biogeochemical component of A_T is generally negligible, except in the Barents Sea Opening where it explains the lack of a significant pH decline (Fig. 7). In our dataset, the effect of changes in temperature on pH in the upper layer is relatively small. In contrast to several studies pointing towards a warming of the Nordic Seas (e.g. Holliday et al., 2008; Blindheim and Østerhus, 2013; Lauvset et al., 2018; Ruiz-Barradas et al., 2018), the Barents Sea Opening, the eastern Fram Strait and the Iceland Sea show no significant change in temperature. This might be an artefact of unequal distribution of sampling over the seasons. When calculating trends with all available temperature data, not only those accompanying the C_T and A_T data, we obtain a clear warming signal (not shown).

In deeper layers, there is an overall increase in C_T, A_T (except in the Iceland Sea), salinity, and temperature. Although the effect of increasing $C_T$bg is reduced away from the surface as a consequence of the gradual isolation of deeper waters from the atmosphere, it remains the main driver of pH change down to 2000 m. The significant trends of $C_T$bg at the 1000-2000 m depth level in the Greenland Sea could be a consequence of the deep winter mixing that has been shown to reach down to 1500 m in this region (Brakstad et al., 2019). In the other regions of the Nordic Seas the winter mixed layers have not been documented to reach these depths (Ólafsson, 2003; Skjelvan et al., 2014; Våge et al., 2015, e.g.). However, intermediate water masses of the Greenland Sea has been shown to spread horizontally in the Nordic Seas, which could also explain the significant trends in the Norwegian and Lofoten Basin and in the Iceland Sea (Blindheim, 1990; Blindheim and Rey, 2004; Messias et al., 2008; Jeansson et al., 2017). The effect of the biogeochemical component of A_T is negligible in deep waters, except for in the Barents Sea Opening, where the increase of $A_T$bg in the 200-500 m layer is as large as in the surface layer, and in the 1000-2000 m layer in the Norwegian Basin, where there is an increase in $A_T$bg that nearly cancels the effect of increasing $C_T$bg. The exceptionally strong trends in $A_T$bg in the upper and the 200-500 m layer in the Barents Sea Opening are intriguing. Considering that the strong $A_T$bg trend also exists in the 200-500 m layer, it is likely not a result of seasonal undersampling. One biogeochemical process that could have a potential impact the Barents Sea $A_T$bg trend is the recurrent blooms of calcifying coccolithophorids (Giraudeau et al., 2016), which consumes A_T during growth, and releases A_T when their shells are decomposed. There are indications of an increase in their presence in the Barents Sea (Giraudeau et al., 2016; Oziel et al., 2020). In which direction this would impact the A_T depends on horizontal advection, remineralization and burial, and deserves separate dedicated process studies. The freshwater components of C_T and A_T are mainly detectable in the upper 500 m. As for the surface, the thermodynamic effect of salinity changes on pH are neglibible in the deep water. The warming seen in deep waters, that has a negative contribution on the pH trend, is an additional indication of that the absence of a temperature trend in the upper layer is a result of seasonal undersampling. In deep waters, the warming signal do not only come from local vertical mixing. There is also an indication of decreased deep-water formation in the Greenland Sea, which has caused an increased exchange with warmer Arctic deep waters (e.g. Østerhus and Gammelsrød, 1999; Blindheim and Rey,

2004; Karstensen et al., 2005; Somavilla et al., 2013). Below 2000 m, there are barely any detectable changes in the various pH drivers. The water masses at these depths are increasingly dominated by old Arctic deep waters (e.g. Somavilla et al., 2013). With ages exceeding 200 years (Jutterström and Jeansson, 2008; Stöven et al., 2016) they have been isolated from the increasing anthropogenic CO_2, which explains the weak trends at these depths.

5.7.2 Past and future drivers

For past and future changes, the drivers of surface pH change show similar spatial patterns over all time periods, except for temperature (Fig. 14). The main driver is an increase in C_T, which is larger in Atlantic Water than in polar waters. This is explained by the dilution of C_T in polar waters by the increased freshwater export from the Arctic Ocean (Fig. 15, Shu et al., 2018) that to some degree counteracts the effect of atmospheric CO_2 uptake. A similar freshwater effect has recently been observed also in the Arctic Ocean (Woosley and Millero, 2020). The biogeochemical component of the C_T driver (Fig. 15), which is primarily the effect of increasing anthropogenic carbon, is larger in polar waters for the changes from present to future in both the esmRCP2.6 and esmRCP8.5 scenarios, in agreement with is what is expected from their lower buffer capacity (Sect. 2). The effect of A_T is most prominent in polar waters, where a reduced A_T concentration contribute to a pH decrease that is of the same order of magnitude as that driven by C_T (Fig. 14). From the freshwater decomposition in Fig. 15, we see that the A_T changes are mainly driven by freshwater fluxes, and that contributions from the biogeochemical component are negligible. A_T dilution has also been shown to be important in the future in the Arctic ocean in several CMIP6-models (Terhaar et al., 2021). However, as discussed earlier, the net effect of these freshwater fluxes on pH are minor, as the dilution of A_T and C_T is similar, but have opposite effects on pH (compare Fig. 15d-f with 15j-k). The increasing freshwater export also results in a dilution of salinity in polar waters that has a positive contribution to the pH trend. The Atlantic Waters show a tendency towards increasing salinity that partly amplifies the decrease in pH. Temperature has an overall negative effect on the pH trend as a result of an overall warming. From pre-industrial to present-day, and present-day to future esmRCP2.6, the temperature increase is almost non-existent in polar waters, indicating that it has been shielded from warming through the presence of sea ice. In some smaller regions there is even a sign of a cooling, which could be a result of an increased presence of polar waters due to the increasing freshwater export.

The combined effect of these drivers explain the zonal gradients in the pH decrease that are described in Sect. 5.3 and 5.5. From past to present-day the largest pH decrease takes place in the Atlantic Water due to a stronger increase of anthropogenic carbon and a stronger warming in these waters. From present-day to future the acidification becomes larger in polar waters compared to Atlantic Water due to the stronger increase of anthropogenic carbon in these waters. The increasing freshwater export from the Arctic that is seen in all time periods is of importance when regarding C_T and A_T concentrations separately, but their combined effect on pH is negligible. For the changes from past to present-day and present-day to future esmRCP2.6 the zonal gradient in Ω_{Ar} trend follows that of pH, showing the importance of the C_T driver. It is reinforced by the spatially variations in the warming, i.e., the stronger warming in the Atlantic Water compared polar waters results in a relatively stronger drop in Ω_{Ar} in polar waters. In the esmRCP8.5 future, Ω_{Ar}, in contrast to pH, exhibit a larger drop in the Atlantic Water. This

can be explained by the relatively small changes in temperature in this region compared to the rest of the Nordic Seas, which affect Ω_{Ar} in the opposite direction compared to pH.

Below the surface layer, C_T is also the main driver of past and future pH changes (Fig. 16). The change from pre-industrial to present-day indicates a gradually weaker impact of C_T with depth, except for a tongue at about 1000 m depth that connects to the surface in the Iceland sea. This is most likely related to the deep water formation in this region that spreads at depth. The end-of-the-century C_T increase for the esmRCP2.6 scenario is larger in the deep than in the surface layer, resulting in the stronger pH reduction at mid-depths as seen in Fig. 10. This mid-depth layer with a strong acidification is partly a result of the higher atmospheric CO_2 concentrations in the middle of the 21st century in combination with the rapid ventilation of the water column in this area, i.e., when these waters were at surface they were exposed to peak atmospheric CO_2. However, the large C_T increase in deep waters is also partly explained by increased remineralization, as indicated by a $\sim$1 ml O_2 l^{-1} increase in the apparent oxygen utilization (AOU) at depths of 1800-2100 m throughout the Nordic Seas in both esmRCP2.6 and esmRCP8.5 (not shown). Assuming a Redfield ratio of O_2:C=132:106, this corresponds to a change in C_T of $\sim$30 μmol kg^{-1}, which results to a pH decrease of $\sim$0.1 at the alkalinity in question. Impacts of changes in A_T, salinity and temperature, are relatively modest at depth.

The residual between the sum of the four drivers and the actual pH change is small (Figs. 14 and 16) and can be attributed to approximations involved in the decomposition, including the approximations of the partial derivatives, the assumption of a linear trend and the use of temporal means (Takahashi et al., 1993; Lenton et al., 2012; Lauvset et al., 2015). Although the absolute numbers related to the drivers should be taken with care, this decomposition still gives a good estimate of the relative importance of temperature, salinity, C_T, and A_T on pH changes.

In the historical run and all three future projections of NorESM1-ME, the change in surface ocean pCO_2 differs from the change in the atmosphere (Fig. S16). From pre-industrial to present-day, there is an increase in the undersaturation, i.e., the increase in the oceanic pCO_2 lags behind the increase in the atmosphere. This means that the pH decrease is less than that expected from the increase in atmospheric CO_2. The lag continues into all the future scenarios, but from around 2040 and onward, the oceanic pCO_2 increases faster than that of the atmosphere, resulting in a decreasing undersaturation. In esmRCP2.6 and esmRCP4.5 this causes stronger decreases in pH (from 1996-2005 to 2090-2099) than expected from the rise in atmospheric CO_2. In esmRCP8.5, however, the difference between the end-of-the century ocean and atmospheric pCO_2 is still larger than the present-day, meaning that the decrease in pH is less than expected. As detailed above there are several mechanisms underlying undersaturation of surface ocean pCO_2 in the Nordic Seas, but further analyses of these, including their potential future changes, is beyond the scope of this paper.

6 Summary and Conclusions

We have provided a detailed analysis of spatial and temporal variations of past, present-day and future acidification, and its drivers, in the Nordic Seas. We have further assessed the potential impacts of this acidification on aragonite saturation and cold-water coral reefs. This work builds on Skjelvan et al. (2014), who estimated pH trends, and their drivers, for various

sub-regions of the Nordic Seas from observational data sampled between 1981 and 2013. Here we have added data from the Iceland Sea and from later years, to obtain the greatest possible temporal and spatial coverage. We have additionally made an analysis of past and future pH changes by the use of the gridded GLODAP climatology and ESM-simulations, to put the observed changes into the context of long-term climate change. In contrast to previous studies that have assessed the future pH changes in the Nordic Seas for single scenarios (Bellerby et al., 2005; Skogen et al., 2014, 2018), we here analyse output from one mitigation scenario, one stabilization scenario and one high-emission scenario. To our knowledge, no previous studies have presented past pH changes in the Nordic Seas.

pH changes and its potential ecosystem impacts

From pre-industrial (1850-1860) to present days (1996-2005), a combination of NorESM1-ME with the GLODAPv2 pre-industrial estimate, suggests that the pH of Nordic Seas surface waters has dropped by 0.1. During this period, the aragonite saturation horizon has slightly shallowed, but has remained well below the depths of known cold-water coral habitats. During 1981-2019, when regular sampling of carbon system variables have been made in the region, the pH of the Nordic Seas upper layer has decreased at a rate of -2.79$\pm$0.3 10^{-3} yr^{-1} on average, resulting in a pH decline of 0.11. The pH reductions are significant all over the Nordic Seas upper layer (0-200 m), except in the Barents Sea Opening where the lack of significant change is a result of a strong increase in A_T. In some regions the acidification is detectable down to 2000 m, which we attribute to the deep water formation and spreading of these water masses at depth. The waters at 1000-2000 m throughout the Nordic Seas are now close to aragonite undersaturation. Our results are in overall agreement with Skjelvan et al. (2014), but the longer timeseries result in statistically significant ($p<0.05$) trends in even more regions and depth layers. An additional pH drop of 0.1-0.4 in the surface waters is projected until the end of the 21st century, depending on the emission scenario. In the high-emission scenario, esmRCP8.5, all cold-water coral reefs will be exposed to corrosive waters by the end of the 21st century, threatening not only their existence, but also that of their associated ecosystems. This is confirmed by an ensemble of 6 CMIP5 models, who all agree on these consequences. The NorESM1-ME simulations suggest that some cold-water corals will be exposed to undersaturation also under the esmRCP4.5 scenario, and that this only can be avoided by keeping the emissions within the limits prescribed in the esmRCP2.6 scenario. Because NorESM1-ME tends to simulate a relatively strong decline of pH and shallow saturation horizons in comparison to our ESM-ensemble for esmRCP8.5, our estimated aragonite saturation horizons for esmRCP2.6 and esmRCP4.5 should be considered as the shallow, lower bound of possible future states. Our estimates of the future pH and Ω_{Ar} in the Nordic Seas add more possible future states to the ones presented for the A1B and RCP4.5 scenarios by Skogen et al. (2014, 2018).

pH drivers

The acidification during the last 39 years is, in all sub-regions, mainly driven by increasing C_T in response to the rising anthropogenic carbon concentrations. This is in agreement with the results for the period of 1981-2013 from Skjelvan et al. (2014), who calculated the drivers of pH change for the Norwegian Basin and the Greenland Sea. The effects of increasing C_T are slightly opposed by increasing A_T. The increasing A_T is partly a result of a "salinification" of the Nordic Seas. However,

this salinification also results in a decrease in C_T, which counteracts the effect of the freshwater-driven increase in A_T. The net effect of C_T and A_T on increasing pH is therefore a result of biogeochemical processes. We find a clear warming signal in deep waters, which has contributed to the decreasing pH. In the upper 200 m, however, there is no clear temperature change. We find this to be a result of seasonal undersampling, which further complicates a comparison of the changes in sea surface pCO_2 to the atmospheric one. In the Barents Sea Opening, there is an exceptionally strong increase in A_T, which we cannot relate to increasing salinity. The reasons behind this strong increase is then either a result of biogeochemical processes, or can also be a result sampling issues. Unfortunately, we cannot pin this down with the dataset we have, and this remains as an open question for future investigations.

For past and future changes, we also find increasing C_T to be the main driver of pH change in the Nordic Seas. This is in agreement with Skogen et al. (2014), but we distinguish some regional differences related to different water masses. Increasing temperatures, that amplifiy the effect of increasing C_T, have the largest impact in Atlantic Water in changes from pre-industrial to present-day and present-day to the future esmRCP2.6. The absence of a warming signal in polar waters is a result of the shielding effect of sea-ice. In esmRCP8.5, however, the warming is more uniform over the Nordic Seas, which most likely is a result of the significantly reduced sea ice cover. In both past and future scenarios, there is a clear signal of an increasing freshwater export from the Arctic Ocean that dilutes C_T, A_T, and salinity in polar waters, and there is a tendency to increasing salinity in the Atlantic Water, that also leads to increasing C_T and A_T. The total effect of this change in freshwater content on pH is negligible as the effect of changing C_T and A_T oppose each other, and because the thermal effect of salinity is minor in comparison to the other drivers.

Data availability. The GLODAPv2.2019 data and GLODAPv2 mapped climatologies are available for download at https://www.glodap.info/index.php/merged-and-adjusted-data-product-v2-2019/ and https://www.glodap.info/index.php/mapped-data-product/ , respectively.

The data from Ocean Weather station M from 2001-2007 is available in GLODAPv2.2019. Data from the time period 2008-2019 will be available in the next GLODAP version.

The data from the time-series station in the Iceland Sea can be obtained from the NCEI database (Ólafsson, 2012; Ólafsdóttir et al., 2020): https://doi.org/10.25921/qhed-3h84, and https://doi.org/10.3334/cdiac/otg.carina_icelandsea.

The data from the Norwegian ocean acidification monitoring program (2011-2012 Tilførselsprogrammet and 2013-2019 Havforsuringsprogrammet) (Chierici et al., 2019a, b), and from the eastern Fram Strait (Chierici and Fransson, 2019) is available at the Norwegian Marine Data Centre (NMDC): http://metadata.nmdc.no/metadata-api/landingpage/17a2f8f382d1f8d47a6f4de44d494fee, http://metadata.nmdc.no/metadata-api/landingpage/46cd81a46f954c864d45445ef20fe504, and https://doi.org/10.21335/NMDC-154415697.

The ESM simulations can be downloaded at https://esgf-node.llnl.gov/search/cmip5/

The cold-water coral positions have been derived from data that is made available under the European Marine Observation Data Network (EMODnet) Seabed Habitats initiative (www.emodnet-seabedhabitats.eu), financed by the European Union under Regulation (EU) No 508/2014 of the European Parliament and of the Council of 15 May 2014 on the European Maritime and Fisheries Fund.

Author contributions. AO, FF and FF designed the research. FF, FF, and AO performed the data-analysis with inputs from NG, IS, MC and EJ. F. Fransner lead the writing of the manuscript with inputs from all co-authors. JT designed, tested, and performed the NorESM1-ME model simulations.

Competing interests. The authors declare that they have no conflict of interest.

Disclaimer. TEXT

Acknowledgements. F. Fransner was funded by the Bjerknes Centre for Climate Research, by the Research Council of Norway through the project The Nansen Legacy (RCN # 276730), and by Det Kongelige Norske Videnskabers Selskap . F. Fröb was funded by the Bjerknes Centre for Climate Research. JT acknowledges funding from the Research Council of Norway (Reef-Futures no. 295340, Columbia no. 275268, and CE2COAST no. 318477). NG acknowledges funding from the Research Council of Norway (IMPOSE, 294930). SKL acknowledges funding from the Research Council of Norway (NorArgo2, 269753). This work is a contribution to the project INTAROS. This project has received funding from the European Union's Horizon 2020 research and innovation programme under grant agreement No 727890. High-performance computing and storage resources were provided by the Norwegian infrastructure for computational science (through projects nn1002k and ns1002k). The Norwegian program "Monitoring ocean acidification in Norwegian waters" is supported by the Norwegian Environmental Agency (no. 17078007). Data from the Barents Sea are supported by Institute of Marine Research and the flagship program "Ocean acidification and ecosystem effects in northern waters" at the FRAM-High North Research Centre for Climate and Environment. We acknowledge the World Climate Research Programme's Working Group on Coupled Modelling, which is responsible for CMIP, and we thank the climate modeling groups for producing and making available their model output. For CMIP, the U.S. Department of Energy's Program for Climate Model Diagnosis and Intercomparison provides coordinating support and led development of software infrastructure in partnership with the Global Organization for Earth System Science Portals. We thank the four reviewers for their constructive feedback that greatly improved the manuscript.

References

Allison, N., Cohen, I., Finch, A., Erez, J., and Tudhope, A.: Corals concentrate dissolved inorganic carbon to facilitate calcification, Nature Communications, 5, https://doi.org/doi:10.1038/ncomms6741, 2014.

Anderson, L. G.: Dissolved inorganic carbon, pH, alkalinity, temperature, salinity and other variables collected from discrete sample and profile observations using CTD, bottle and other instruments from the LANCE in the Barents Sea from 1986-07-19 to 1986-07-26 (NCEI Accession 0113910). NOAA National Centers for Environmental Information. Dataset., https://doi.org/10.3334/cdiac/otg.carina_58la19860719, dataset, 2013a.

Anderson, L. G.: Dissolved inorganic carbon, pH, alkalinity, temperature, salinity and other variables collected from discrete sample and profile observations using CTD, bottle and other instruments from the ODEN in the Arctic Ocean, Barents Sea and others from 2002-04-20 to 2002-06-06 (NCEI Accession 0113590). NOAA National Centers for Environmental Information., https://doi.org/10.3334/cdiac/otg.carina_77dn20020420, dataset, 2013b.

Anderson, L. G. and Olsen, A.: Air–sea flux of anthropogenic carbon dioxide in the North Atlantic, Geophysical Research Letters, 29, 16–1–16–4, https://doi.org/10.1029/2002GL014820, https://agupubs.onlinelibrary.wiley.com/doi/abs/10.1029/2002GL014820, 2002.

Anderson, L. G., Blindheim, J., and Rey, F.: Dissolved inorganic carbon, pH, alkalinity, temperature, salinity and other variables collected from discrete sample and profile observations using CTD, bottle and other instruments from the JOHAN HJORT in the North Greenland Sea and Norwegian Sea from 1997-04-14 to 1997-05-22 (NCEI Accession 0113563). NOAA National Centers for Environmental Information., https://doi.org/10.3334/cdiac/otg.carina_58jh19970414, dataset, 2013a.

Anderson, L. G., Johannessen, T., and Rey, F.: Dissolved inorganic carbon, pH, alkalinity, temperature, salinity and other variables collected from discrete sample and profile observations using CTD, bottle and other instruments from the JOHAN HJORT in the North Greenland Sea and Norwegian Sea from 1998-08-01 to 1998-08-23 (NCEI Accession 0113758). NOAA National Centers for Environmental Information., https://doi.org/10.3334/cdiac/otg.carina_58jh19980801, dataset, 2013b.

Arora, V. K., Scinocca, J. F., Boer, G. J., Christian, J. R., Denman, K. L., Flato, G. M., Kharin, V. V., Lee, W. G., and Merryfield, W. J.: Carbon emission limits required to satisfy future representative concentration pathways of greenhouse gases, Geophysical Research Letters, 38, https://doi.org/https://doi.org/10.1029/2010GL046270, https://agupubs.onlinelibrary.wiley.com/doi/abs/10.1029/2010GL046270, 2011.

Bellerby, R. G. J. and Smethie, William M., J.: Dissolved inorganic carbon, alkalinity, temperature, salinity and other variables collected from discrete sample and profile observations using CTD, bottle and other instruments from the KNORR in the Barents Sea, North Atlantic Ocean and others from 2002-05-30 to 2002-07-01 (NCEI Accession 0113569). NOAA National Centers for Environmental Information., https://doi.org/10.3334/cdiac/otg.carina_316n20020530, dataset, 2013.

Bellerby, R. G. J., Olsen, A., Furevik, T., and Anderson, L. G.: Response of the Surface Ocean CO2 System in the Nordic Seas and Northern North Atlantic to Climate Change, pp. 189–197, American Geophysical Union (AGU), https://doi.org/https://doi.org/10.1029/158GM13, https://agupubs.onlinelibrary.wiley.com/doi/abs/10.1029/158GM13, 2005.

Bentsen, M., Bethke, I., Debernard, J. B., Iversen, T., Kirkevåg, A., Seland, Ø., Drange, H., Roelandt, C., Seierstad, I. A., Hoose, C., and Kristjánsson, J. E.: The Norwegian Earth System Model, NorESM1-M – Part 1: Description and basic evaluation of the physical climate, Geoscientific Model Development, 6, 687–720, https://doi.org/10.5194/gmd-6-687-2013, https://gmd.copernicus.org/articles/6/687/2013/, 2013.

Bleck, R. and Smith, L. T.: A wind-driven isopycnic coordinate model of the north and equatorial Atlantic Ocean: 1. Model development and supporting experiments, Journal of Geophysical Research: Oceans, 95, 3273–3285, https://doi.org/10.1029/JC095iC03p03273, https://agupubs.onlinelibrary.wiley.com/doi/abs/10.1029/JC095iC03p03273, 1990.

Blindheim, J.: Arctic intermediate water in the Norwegian sea, Deep Sea Research Part A. Oceanographic Research Papers, 37, 1475 – 1489, https://doi.org/https://doi.org/10.1016/0198-0149(90)90138-L, http://www.sciencedirect.com/science/article/pii/019801499090138L, 1990.

Blindheim, J. and Østerhus, S.: The Nordic Seas, Main Oceanographic Features, pp. 11–37, American Geophysical Union (AGU), https://doi.org/10.1029/158GM03, https://agupubs.onlinelibrary.wiley.com/doi/abs/10.1029/158GM03, 2013.

Blindheim, J. and Rey, F.: Water-mass formation and distribution in the Nordic Seas during the 1990s, ICES Journal of Marine Science, 61, 846–863, https://doi.org/10.1016/j.icesjms.2004.05.003, https://doi.org/10.1016/j.icesjms.2004.05.003, 2004.

Bockmon, E. E. and Dickson, A. G.: An inter-laboratory comparison assessing the quality of seawater carbon dioxide measurements, Marine Chemistry, 171, 36–43, https://doi.org/https://doi.org/10.1016/j.marchem.2015.02.002, https://www.sciencedirect.com/science/article/pii/S0304420315000213, 2015.

Booth, B. B. B., Bernie, D., McNeall, D., Hawkins, E., Caesar, J., Boulton, C., Friedlingstein, P., and Sexton, D. M. H.: Scenario and modelling uncertainty in global mean temperature change derived from emission-driven global climate models, Earth System Dynamics, 4, 95–108, https://doi.org/10.5194/esd-4-95-2013, https://esd.copernicus.org/articles/4/95/2013/, 2013.

Bopp, L., Resplandy, L., Orr, J. C., Doney, S. C., Dunne, J. P., Gehlen, M., Halloran, P., Heinze, C., Ilyina, T., Séférian, R., Tjiputra, J., and Vichi, M.: Multiple stressors of ocean ecosystems in the 21st century: projections with CMIP5 models, Biogeosciences, 10, 6225–6245, https://doi.org/10.5194/bg-10-6225-2013, https://bg.copernicus.org/articles/10/6225/2013/, 2013.

Brakstad, A., Våge, K., Håvik, L., and Moore, G. W. K.: Water Mass Transformation in the Greenland Sea during the Period 1986–2016, Journal of Physical Oceanography, 49, 121–140, https://doi.org/10.1175/JPO-D-17-0273.1, https://doi.org/10.1175/JPO-D-17-0273.1, 2019.

Brewer, P. G., Takahashi, T., and Williams, R. T.: Partial pressure (or fugacity) of carbon dioxide, dissolved inorganic carbon (DIC), total alkalinity, water temperature, salinity, dissolved oxygen concentration and other variables collected from discrete sample and profile observations during R/V Knorr TTO-NAS cruises in the North Atlantic Ocean from 1981-04-01 to 1981-10-19 (NCEI Accession 0000733). NOAA National Centers for Environmental Information., https://doi.org/10.3334/cdiac/otg.ndp004, dataset, 2010.

Buhl-Mortensen, L., Olafsdottir, S. H., Buhl-Mortensen, P., Burgos, J. M., and Ragnarsson, S. A.: Distribution of nine cold-water coral species (Scleractinia and Gorgonacea) in the cold temperate North Atlantic: effects of bathymetry and hydrography, Hydrobiologia, 759, 39–61, https://doi.org/10.1007/s10750-014-2116-x, https://doi.org/10.1007/s10750-014-2116-x, 2015.

Caldeira, K. and Wickett, M. E.: Anthropogenic carbon and ocean pH, Nature, 425, 365–365, https://doi.org/10.1038/425365a, https://doi.org/10.1038/425365a, 2003.

Chafik, L. and Rossby, T.: Volume, Heat, and Freshwater Divergences in the Subpolar North Atlantic Suggest the Nordic Seas as Key to the State of the Meridional Overturning Circulation, Geophysical Research Letters, 46, 4799–4808, https://doi.org/10.1029/2019GL082110, https://agupubs.onlinelibrary.wiley.com/doi/abs/10.1029/2019GL082110, 2019.

Chierici, M. and Fransson, A.: Seasonal variability of the marine CO_2 system and nutrients in the Atlantic water inflow to the Arctic Ocean in 2014, https://doi.org/10.21335/NMDC-154415697, dataset, 2019.

Chierici, M., Sørensen, K., Johannessen, T., Børsheim, K., A.Olsen, Yakushev, E., Omar, A., and Blakseth, T.: Tillførselprogrammet 2011, Overvåking av havsforsuring av norske farvann. Rapport, Klif, TA2936-2012, Tech. rep., 2012.

Chierici, M., Sørensen, K., Johannessen, T., Børsheim, K., A.Olsen, Yakushev, E., Omar, A., Skjelvan, I., Norli, M., , and Lauvset, S.: Tillførselprogrammet 2012, Overvåking av havsforsuring av norske farvann. Rapport, Klif, TA3043-2013, Tech. rep., 2013.

Chierici, M., Skjelvan, I., Bellerby, R., M. Norli, L. F., Hodal, H., Børsheim, K., Lauvset, S., Johannessen, T., Sørensen, K., and Yakushev, E.: Overvåking av havforsuring av norske farvann. Rapport, Miljødirektoratet M-218, Tech. rep., 2014.

Chierici, M., Skjelvan, I., Norli, M., Lødemel, H., Lunde, L., Sørensen, K., Yakushev, E., Bellerby, R., King, A., Lauvset, S., Johannessen, T., and Børsheim, K.: Overvåking av havforsuring i norske farvann i 2014, Rapport, Miljødirektoratet, M-354, Tech. rep., 2015.

Chierici, M., Skjelvan, I., Norli, M., Børsheim, K., Lauvset, S., Lødemel, H., Sørensen, K., King, A., Kutti, T., Renner, A., Omar, A., and Johannessen, T.: Overvåking av havforsuring i norske farvann i 2015, Rapport, Miljødirektoratet, M-573, Tech. rep., 2016.

Chierici, M., Skjelvan, I., Norli, M., Jones, E., Børsheim, K., Lauvset, S., Lødemel, H., Sørensen, K., King, A., and Johannessen, T.: Overvåking av havforsuring i norske farvann i 2016, Rapport, Miljødirektoratet, M-776, Tech. rep., 2017.

Chierici, M., Jones, E., and Lødemel, H. H.: Interannual variability of the marine CO_2 system and nutrients in the Barents Sea from 2011 to 2017, https://doi.org/10.21335/NMDC-1738969988, dataset, 2019a.

Chierici, M., Jones, E., and Lødemel, H. H.: Interannual variability of the marine CO_2 system and nutrients in the Norwegian Sea from 2011 to 2017, https://doi.org/10.21335/NMDC-1939716216, dataset, 2019b.

Chierici, M., Vernet, M., Fransson, A., and Børsheim, K. Y.: Net Community Production and Carbon Exchange From Winter to Summer in the Atlantic Water Inflow to the Arctic Ocean, Frontiers in Marine Science, 6, 528, https://doi.org/10.3389/fmars.2019.00528, https://www.frontiersin.org/article/10.3389/fmars.2019.00528, 2019c.

Dickson, A., Sabine, C., and Christian, J. e.: Guide to best practices for ocean CO2 measurement., PICES Special Publication 3; IOCCP Report 8, 2007.

Dickson, A. G.: Standard potential of the reaction: AgCl(s) + 12H2(g) = Ag(s) + HCl(aq), and and the standard acidity constant of the ion HSO4- in synthetic sea water from 273.15 to 318.15 K, The Journal of Chemical Thermodynamics, 22, 113 – 127, https://doi.org/https://doi.org/10.1016/0021-9614(90)90074-Z, http://www.sciencedirect.com/science/article/pii/002196149090074Z, 1990.

Dickson, R. R. and Brown, J.: The production of North Atlantic Deep Water: Sources, rates, and pathways, Journal of Geophysical Research: Oceans, 99, 12 319–12 341, https://doi.org/10.1029/94JC00530, https://agupubs.onlinelibrary.wiley.com/doi/abs/10.1029/94JC00530, 1994.

Doney, S. C., Fabry, V. J., Feely, R. A., and Kleypas, J. A.: Ocean Acidification: The Other CO_2 Problem, Annual Review of Marine Science, 1, 169–192, https://doi.org/10.1146/annurev.marine.010908.163834, https://doi.org/10.1146/annurev.marine.010908.163834, pMID: 21141034, 2009.

Doney, S. C., Busch, D. S., Cooley, S. R., and Kroeker, K. J.: The Impacts of Ocean Acidification on Marine Ecosystems and Reliant Human Communities, Annual Review of Environment and Resources, 45, null, https://doi.org/10.1146/annurev-environ-012320-083019, https://doi.org/10.1146/annurev-environ-012320-083019, 2020.

Doo, S. S., Kealoha, A., Andersson, A., Cohen, A. L., Hicks, T. L., Johnson, Z. I., Long, M. H., McElhany, P., Mollica, N., Shamberger, K. E. F., Silbiger, N. J., Takeshita, Y., and Busch, D. S.: The challenges of detecting and attributing ocean acidification impacts on marine ecosystems, ICES Journal of Marine Science, https://doi.org/10.1093/icesjms/fsaa094, https://doi.org/10.1093/icesjms/fsaa094, fsaa094, 2020.

Dufresne, J.-L., Foujols, M.-A., Denvil, S., Caubel, A., Marti, O., Aumont, O., Balkanski, Y., Bekki, S., Bellenger, H., Benshila, R., Bony, S., Bopp, L., Braconnot, P., Brockmann, P., Cadule, P., Cheruy, F., Codron, F., Cozic, A., Cugnet, D., de Noblet, N., Duvel, J.-P., Ethé, P.,

Fairhead, L., Fichefet, T., Flavoni, S., Friedlingstein, P., Grandpeix, J.-Y., Guez, L., Guilyardi, E., Hauglustaine, D., Hourdin, F., Idelkadi, A., Ghattas, J., Joussaume, S., Kageyama, M., Krinner, G., Labetoulle, S., Lahellec, A., Lefebvre, M.-P., Lefevre, F., Levy, C., Li, Z. X., Lloyd, J., Lott, F., Madec, G., Mancip, M., Marchand, M., Masson, S., Meurdesoif, Y., Mignot, J., Musat, I., Parouty, S., Polcher, J., Rio, C., Schulz, M., Swingedouw, D., Szopa, S., Talandier, C., Terray, P., Viovy, N., and Vuichard, N.: Climate change projections using the IPSL-CM5 Earth System Model: from CMIP3 to CMIP5, Clim. Dynamics, 40, 2123–2165, https://doi.org/10.1007/s00382-012-1636-1, 2013.

Dunne, J. P., John, J. G., Adcroft, A. J., Griffies, S. M., Hallberg, R. W., Shevliakova, E. N., Stouffer, R. J., Cooke, W., Dunne, K. A., Harrison, M. J., Krasting, J. P., Malyshev, S. L., Milly, P. C. D., Phillips, P. J., Sentman, L. T., Samuels, B. L., Spelman, M., Winton, M., Wittenberg, A. T., and Zadeh, N.: GFDL's ESM2 global coupled climate-carbon Earth System Models Part I: Physical Formulation and Baseline Simulation Characteristics, J. Climate, 25, https://doi.org/10.1175/JCLI-D-11-00560.1, 2013a.

Dunne, J. P., John, J. G., Adcroft, A. J., Griffies, S. M., Hallberg, R. W., Shevliakova, E. N., Stouffer, R. J., Cooke, W., Dunne, K. A., Harrison, M. J., Krasting, J. P., Malyshev, S. L., Milly, P. C. D., Phillips, P. J., Sentman, L. T., Samuels, B. L., Spelman, M., Winton, M., Wittenberg, A. T., and Zadeh, N.: GFDL's ESM2 global coupled climate-carbon Earth System Models Part II: Carbon System Formulation and Baseline Simulation Characteristics, J. Climate, 26, https://doi.org/10.1175/JCLI-D-12-00150.1, 2013b.

Fassbender, A. J., Sabine, C. L., and Palevsky, H. I.: Nonuniform ocean acidification and attenuation of the ocean carbon sink, Geophysical Research Letters, 44, 8404–8413, https://doi.org/https://doi.org/10.1002/2017GL074389, https://agupubs.onlinelibrary.wiley.com/doi/abs/10.1002/2017GL074389, 2017.

Fassbender, A. J., Orr, J. C., and Dickson, A. G.: Technical note: Interpreting pH changes, Biogeosciences, 18, 1407–1415, https://doi.org/10.5194/bg-18-1407-2021, https://bg.copernicus.org/articles/18/1407/2021/, 2021.

Frankignoulle, M.: A complete set of buffer factors for acid/base CO2 system in seawater, Journal of Marine Systems, 5, 111–118, https://doi.org/https://doi.org/10.1016/0924-7963(94)90026-4, https://www.sciencedirect.com/science/article/pii/0924796394900264, 1994.

Friedlingstein, P., Meinshausen, M., Arora, V. K., Jones, C. D., Anav, A., Liddicoat, S. K., and Knutti, R.: Uncertainties in CMIP5 Climate Projections due to Carbon Cycle Feedbacks, Journal of Climate, 27, 511 – 526, https://doi.org/10.1175/JCLI-D-12-00579.1, https://journals.ametsoc.org/view/journals/clim/27/2/jcli-d-12-00579.1.xml, 2014.

Friedlingstein, P., O'Sullivan, M., Jones, M. W., Andrew, R. M., Hauck, J., Olsen, A., Peters, G. P., Peters, W., Pongratz, J., Sitch, S., Le Quéré, C., Canadell, J. G., Ciais, P., Jackson, R. B., Alin, S., Aragão, L. E. O. C., Arneth, A., Arora, V., Bates, N. R., Becker, M., Benoit-Cattin, A., Bittig, H. C., Bopp, L., Bultan, S., Chandra, N., Chevallier, F., Chini, L. P., Evans, W., Florentie, L., Forster, P. M., Gasser, T., Gehlen, M., Gilfillan, D., Gkritzalis, T., Gregor, L., Gruber, N., Harris, I., Hartung, K., Haverd, V., Houghton, R. A., Ilyina, T., Jain, A. K., Joetzjer, E., Kadono, K., Kato, E., Kitidis, V., Korsbakken, J. I., Landschützer, P., Lefèvre, N., Lenton, A., Lienert, S., Liu, Z., Lombardozzi, D., Marland, G., Metzl, N., Munro, D. R., Nabel, J. E. M. S., Nakaoka, S.-I., Niwa, Y., O'Brien, K., Ono, T., Palmer, P. I., Pierrot, D., Poulter, B., Resplandy, L., Robertson, E., Rödenbeck, C., Schwinger, J., Séférian, R., Skjelvan, I., Smith, A. J. P., Sutton, A. J., Tanhua, T., Tans, P. P., Tian, H., Tilbrook, B., van der Werf, G., Vuichard, N., Walker, A. P., Wanninkhof, R., Watson, A. J., Willis, D., Wiltshire, A. J., Yuan, W., Yue, X., and Zaehle, S.: Global Carbon Budget 2020, Earth System Science Data, 12, 3269–3340, https://doi.org/10.5194/essd-12-3269-2020, https://essd.copernicus.org/articles/12/3269/2020/, 2020.

Friis, K., Körtzinger, A., and Wallace, D. W. R.: The salinity normalization of marine inorganic carbon chemistry data, Geophysical Research Letters, 30, https://doi.org/https://doi.org/10.1029/2002GL015898, https://agupubs.onlinelibrary.wiley.com/doi/abs/10.1029/2002GL015898, 2003.

Fröb, F., Olsen, A., Becker, M., Chafik, L., Johannessen, T., Reverdin, G., and Omar, A.: Wintertime fCO2 Variability in the Subpolar North Atlantic Since 2004, Geophysical Research Letters, 46, 1580–1590, https://doi.org/https://doi.org/10.1029/2018GL080554, https://agupubs.onlinelibrary.wiley.com/doi/abs/10.1029/2018GL080554, 2019.

Frölicher, T. L., Rodgers, K. B., Stock, C. A., and Cheung, W. W. L.: Sources of uncertainties in 21st century projections of potential ocean ecosystem stressors, Global Biogeochemical Cycles, 30, 1224–1243, https://doi.org/https://doi.org/10.1002/2015GB005338, https://agupubs.onlinelibrary.wiley.com/doi/abs/10.1002/2015GB005338, 2016.

García-Ibáñez, M. I., Bates, N. R., Bakker, D. C., Fontela, M., and Velo, A.: Cold-water corals in the Subpolar North Atlantic Ocean exposed to aragonite undersaturation if the 2 °C global warming target is not met, Global and Planetary Change, 201, 103 480, https://doi.org/https://doi.org/10.1016/j.gloplacha.2021.103480, https://www.sciencedirect.com/science/article/pii/S0921818121000655, 2021.

Gattuso, J.-P. and Hansson, L.: Ocean acidification: background and history, In Ocean Acidification, ed. J-P Gattuso, L Hansson, pp. 1–20, Oxford University Press, Oxford, UK, 2011.

Giorgetta, M. A., Jungclaus, J., Reick, C. H., Legutke, S., Bader, J., Böttinger, M., Brovkin, V., Crueger, T., Esch, M., Fieg, K., Glushak, K., Gayler, V., Haak, H., Hollweg, H.-D., Ilyina, T., Kinne, S., Kornblueh, L., Matei, D., Mauritsen, T., Mikolajewicz, U., Mueller, W., Notz, D., Pithan, F., Raddatz, T., Rast, S., Redler, R., Roeckner, E., Schmidt, H., Schnur, R., Segschneider, J., Six, K. D., Stockhause, M., Timmreck, C., Wegner, J., Widmann, H., Wieners, K.-H., Claussen, M., Marotzke, J., and Stevens, B.: Climate and carbon cycle changes from 1850 to 2100 in MPI-ESM simulations for the Coupled Model Intercomparison Project phase 5, Journal of Advances in Modeling Earth Systems, 5, 572–597, https://doi.org/10.1002/jame.20038, 2013.

Giraudeau, J., Hulot, V., Hanquiez, V., Devaux, L., Howa, H., and Garlan, T.: A survey of the summer coccolithophore community in the western Barents Sea, Journal of Marine Systems, 158, 93–105, https://doi.org/https://doi.org/10.1016/j.jmarsys.2016.02.012, https://www.sciencedirect.com/science/article/pii/S0924796316300021, 2016.

Guinotte, J. M., Orr, J., Cairns, S., Freiwald, A., Morgan, L., and George, R.: Will human-induced changes in seawater chemistry alter the distribution of deep-sea scleractinian corals?, Frontiers in Ecology and the Environment, 4, 141–146, https://doi.org/10.1890/1540-9295(2006)004[0141:WHCISC]2.0.CO;2, 2006.

He, Y.-C., Tjiputra, J., Langehaug, H. R., Jeansson, E., Gao, Y., Schwinger, J., and Olsen, A.: A Model-Based Evaluation of the Inverse Gaussian Transit-Time Distribution Method for Inferring Anthropogenic Carbon Storage in the Ocean, Journal of Geophysical Research: Oceans, 123, 1777–1800, https://doi.org/https://doi.org/10.1002/2017JC013504, https://agupubs.onlinelibrary.wiley.com/doi/abs/10.1002/2017JC013504, 2018.

Hennige, S. J., Wicks, L. C., Kamenos, N. A., Perna, G., Findlay, H. S., and Roberts, J. M.: Hidden impacts of ocean acidification to live and dead coral framework, Proceedings of the Royal Society B: Biological Sciences, 282, 20150 990, https://doi.org/10.1098/rspb.2015.0990, https://royalsocietypublishing.org/doi/abs/10.1098/rspb.2015.0990, 2015.

Holliday, N. P., Hughes, S. L., Bacon, S., Beszczynska-Möller, A., Hansen, B., Lavín, A., Loeng, H., Mork, K. A., Østerhus, S., Sherwin, T., and Walczowski, W.: Reversal of the 1960s to 1990s freshening trend in the northeast North Atlantic and Nordic Seas, Geophysical Research Letters, 35, https://doi.org/10.1029/2007GL032675, https://agupubs.onlinelibrary.wiley.com/doi/abs/10.1029/2007GL032675, 2008.

Jeansson, E., Olsen, A., Eldevik, T., Skjelvan, I., Omar, A. M., Lauvset, S. K., Nilsen, J. E. Ø., Bellerby, R. G. J., Johannessen, T., and Falck, E.: The Nordic Seas carbon budget: Sources, sinks, and uncertainties, Global Biogeochemical Cycles, 25, https://doi.org/10.1029/2010GB003961, https://agupubs.onlinelibrary.wiley.com/doi/abs/10.1029/2010GB003961, 2011.

Jeansson, E., Olsen, A., and Jutterström, S.: Arctic Intermediate Water in the Nordic Seas, 1991–2009, Deep Sea Research Part I: Oceanographic Research Papers, 128, 82 – 97, https://doi.org/https://doi.org/10.1016/j.dsr.2017.08.013, http://www.sciencedirect.com/science/article/pii/S0967063716300668, 2017.

Jeansson, E., Olsen, A., Lauvset, S. K., Brakstad, A., Jackson, K., Lunde, L. F., He, Y., and Onarheim, T.: Discrete profile measurements of dissolved inorganic carbon, total alkalinity, other hydrographic and chemical data obtained during the R/V G.O. Sars Repeat Hydrography Cruise in the Greenland Sea and Iceland Sea: GO-SHIP Section 75N (EXPOCODE 58GS20160802), from 2016-08-02 to 2016-08-12 (NCEI Accession 0174834). NOAA National Centers for Environmental Information., https://doi.org/10.25921/3kjg-ak47., dataset, 2018.

Jiang, L.-Q., Carter, B. R., Feely, R. A., Lauvset, S. K., and Olsen, A.: Surface ocean pH and buffer capacity: past, present and future, Scientific Reports, 9, 18 624, https://doi.org/10.1038/s41598-019-55039-4, https://doi.org/10.1038/s41598-019-55039-4, 2019.

Johannessen, T.: Dissolved inorganic carbon, alkalinity, temperature, salinity and other variables collected from discrete sample and profile observations using CTD, bottle and other instruments from the HAKON MOSBY in the North Greenland Sea from 1996-11-21 to 1996-11-30 (NCEI Accession 0113544). NOAA National Centers for Environmental Information., https://doi.org/10.3334/cdiac/otg.carina_58aa19961121, dataset, 2013a.

Johannessen, T.: Dissolved inorganic carbon, alkalinity, temperature, salinity and other variables collected from discrete sample and profile observations using CTD, bottle and other instruments from the HAKON MOSBY in the North Greenland Sea and Norwegian Sea from 1997-02-25 to 1997-03-24 (NCEI Accession 0113545). NOAA National Centers for Environmental Information., https://doi.org/10.3334/cdiac/otg.carina_58aa19970225, dataset, 2013b.

Johannessen, T. and Golmen, L. G.: Dissolved inorganic carbon, alkalinity, temperature, salinity and other variables collected from discrete sample and profile observations using CTD, bottle and other instruments from the HAKON MOSBY in the North Greenland Sea and Norwegian Sea from 1994-08-26 to 1994-09-10 (NCEI Accession 0113542). NOAA National Centers for Environmental Information., https://doi.org/10.3334/cdiac/otg.carina_58aa19940826, dataset, 2013.

Johannessen, T. and Olsen, A.: Dissolved inorganic carbon, alkalinity, temperature, salinity and other variables collected from discrete sample and profile observations during the G.O. SARS cruise along GO-SHIP Repeat Section A75N (EXPOCODE 58GS200309) in the North Atlantic Ocean, North Greenland Sea and Norwegian Sea from 2003-09-22 to 2003-10-13 (NCEI Accession 0113752). NOAA National Centers for Environmental Information., https://doi.org/10.3334/cdiac/otg.carina_58gs20030922, dataset, 2013.

Johannessen, T. and Simonsen, K. .: Dissolved inorganic carbon, alkalinity, temperature, salinity and other variables collected from discrete sample and profile observations using CTD, bottle and other instruments from the HAKON MOSBY in the North Greenland Sea and Norwegian Sea from 1998-03-08 to 1998-03-24 (NCEI Accession 0113546). NOAA National Centers for Environmental Information., https://doi.org/10.3334/cdiac/otg.carina_58aa19980308, dataset, 2013.

Johannessen, T., Skjelvan, I., and Rey, F.: Dissolved inorganic carbon, alkalinity, temperature, salinity and other variables collected from discrete sample and profile observations using CTD, bottle and other instruments from the JOHAN HJORT in the North Greenland Sea and Norwegian Sea from 1994-05-25 to 1994-06-06 (NCEI Accession 0113954). NOAA National Centers for Environmental Information., https://doi.org/10.3334/cdiac/otg.carina_58jh19940525, dataset, 2013a.

Johannessen, T., Skjelvan, I., and Watson, A. J.: Dissolved inorganic carbon, alkalinity, temperature, salinity and other variables collected from discrete sample and profile observations using CTD, bottle and other instruments from the JAMES CLARK ROSS in the North Greenland Sea and Norwegian Sea from 1996-07-20 to 1996-08-22 (NCEI Accession 0113757). NOAA National Centers for Environmental Information. Dataset., https://doi.org/10.3334/cdiac/otg.carina_74jc19960720., dataset, 2013b.

Johannessen, T., Soiland, H., Thingstad, T. F., Bellerby, R. G. J., and Olsen, A.: Dissolved inorganic carbon, alkalinity, temperature, salinity and other variables collected from discrete sample and profile observations using CTD, bottle and other instruments from the G.O. SARS in the Barents Sea, North Atlantic Ocean and others from 2009-05-28 to 2009-08-11 (NCEI Accession 0114433). NOAA National Centers for Environmental Information., https://doi.org/10.25921/3q88-gs40, dataset, 2013c.

Jones, E., Chierici, M., Skjelvan, I., M. Norli, K. B., Lødemel, H., Kutti, T., Sørensen, K., King, A., Jackson, K., and de Lange, T.: Monitoring of the ocean acidification in Norwegian seas in 2017, Report, Miljødirektoratet, M-1072, Tech. rep., 2018.

Jones, E., Chierici, M., Skjelvan, I., Norli, M., Børsheim, K., Lødemel, H., Sørensen, K., King, A., Lauvset, S., Jackson, K., de Lange, T., Johannsessen, T., and Mourgues, C.: Monitoring ocean acidification in Norwegian seas in 2018, Rapport, Miljødirektoratet, M-1417, Tech. rep., 2019.

Jones, E., Chierici, M., Skjelvan, I., Norli, M., Frigstad, H., Børsheim, K., Lødemel, H., Kutti, T., King, A., Sørensen, K., Lauvset, S., Jackson-Misje, K., Apelthun, L., de Lange, T., Johannsessen, T., Mourgues, C., and Bellerby, R.: Monitoring ocean acidification in Norwegian seas in 2019, Rapport, Miljødirektoratet, M-1735, Tech. rep., 2020.

Jones, E. P., Azetsu-Scott, K., Aagaard, K., Carmack, E., and Swift, J. H.: Dissolved inorganic carbon, alkalinity, temperature, salinity and other variables collected from discrete sample and profile observations using CTD, bottle and other instruments from the LOUIS S. ST. LAURENT in the Arctic Ocean, Beaufort Sea and North Greenland Sea from 1994-07-24 to 1994-09-01 (NCEI Accession 0113983).NOAA National Centers for Environmental Information., https://doi.org/10.3334/cdiac/otg.carina_18sn19940724, dataset, 2013.

Jutterström, S. and Jeansson, E.: Anthropogenic carbon in the East Greenland Current, Progress in Oceanography, 78, 29 – 36, https://doi.org/https://doi.org/10.1016/j.pocean.2008.04.001, http://www.sciencedirect.com/science/article/pii/S0079661108000876, 2008.

Karstensen, J., Schlosser, P., Wallace, D. W. R., Bullister, J. L., and Blindheim, J.: Water mass transformation in the Greenland Sea during the 1990s, Journal of Geophysical Research: Oceans, 110, https://doi.org/https://doi.org/10.1029/2004JC002510, https://agupubs.onlinelibrary.wiley.com/doi/abs/10.1029/2004JC002510, 2005.

Keeling, C. D., Brix, H., and Gruber, N.: Seasonal and long-term dynamics of the upper ocean carbon cycle at Station ALOHA near Hawaii, Global Biogeochemical Cycles, 18, https://doi.org/https://doi.org/10.1029/2004GB002227, https://agupubs.onlinelibrary.wiley.com/doi/abs/10.1029/2004GB002227, 2004.

Kutti, T., Bergstad, O. A., Fosså, J. H., and Helle, K.: Cold-water coral mounds and sponge-beds as habitats for demersal fish on the Norwegian shelf, Deep Sea Research Part II: Topical Studies in Oceanography, 99, 122 – 133, https://doi.org/https://doi.org/10.1016/j.dsr2.2013.07.021, http://www.sciencedirect.com/science/article/pii/S0967064513002956, biology and Geology of Deep-Sea Coral Ecosystems: Proceedings of the Fifth International Symposium on Deep Sea Corals, 2014.

Kwiatkowski, L., Torres, O., Bopp, L., Aumont, O., Chamberlain, M., Christian, J. R., Dunne, J. P., Gehlen, M., Ilyina, T., John, J. G., Lenton, A., Li, H., Lovenduski, N. S., Orr, J. C., Palmieri, J., Santana-Falcón, Y., Schwinger, J., Séférian, R., Stock, C. A., Tagliabue, A., Takano, Y., Tjiputra, J., Toyama, K., Tsujino, H., Watanabe, M., Yamamoto, A., Yool, A., and Ziehn, T.: Twenty-first century ocean warming, acidification, deoxygenation, and upper-ocean nutrient and primary production decline from CMIP6 model projections, Biogeosciences, 17, 3439–3470, https://doi.org/10.5194/bg-17-3439-2020, https://bg.copernicus.org/articles/17/3439/2020/, 2020.

Lauvset, S. K., Gruber, N., Landschützer, P., Olsen, A., and Tjiputra, J.: Trends and drivers in global surface ocean pH over the past 3 decades, Biogeosciences, 12, 1285–1298, https://doi.org/10.5194/bg-12-1285-2015, https://bg.copernicus.org/articles/12/1285/2015/, 2015.

Lauvset, S. K., Key, R. M., Olsen, A., van Heuven, S., Velo, A., Lin, X., Schirnick, C., Kozyr, A., Tanhua, T., Hoppema, M., Jutterström, S., Steinfeldt, R., Jeansson, E., Ishii, M., Perez, F. F., Suzuki, T., and Watelet, S.: A new global interior ocean mapped climatology: the $1^\circ \times 1^\circ$ GLODAP version 2, Earth System Science Data, 8, 325–340, https://doi.org/10.5194/essd-8-325-2016, https://essd.copernicus.org/articles/8/325/2016/, 2016.

Lauvset, S. K., Brakstad, A., Våge, K., Olsen, A., Jeansson, E., and Mork, K. A.: Continued warming, salinification and oxygenation of the Greenland Sea gyre, Tellus A: Dynamic Meteorology and Oceanography, 70, 1–9, https://doi.org/10.1080/16000870.2018.1476434, https://doi.org/10.1080/16000870.2018.1476434, 2018.

Lauvset, S. K., Carter, B. R., Pèrez, F. F., Jiang, L.-Q., Feely, R. A., Velo, A., and Olsen, A.: Processes Driving Global Interior Ocean pH Distribution, Global Biogeochemical Cycles, 34, e2019GB006 229, https://doi.org/https://doi.org/10.1029/2019GB006229, https://agupubs.onlinelibrary.wiley.com/doi/abs/10.1029/2019GB006229, e2019GB006229 2019GB006229, 2020.

Lefèvre, N., Watson, A. J., Olsen, A., Ríos, A. F., Pérez, F. F., and Johannessen, T.: A decrease in the sink for atmospheric CO_2 in the North Atlantic, Geophysical Research Letters, 31, https://doi.org/10.1029/2003GL018957, https://agupubs.onlinelibrary.wiley.com/doi/abs/10.1029/2003GL018957, 2004.

Lenton, A., Metzl, N., Takahashi, T., Kuchinke, M., Matear, R. J., Roy, T., Sutherland, S. C., Sweeney, C., and Tilbrook, B.: The observed evolution of oceanic pCO2 and its drivers over the last two decades, Global Biogeochemical Cycles, 26, https://doi.org/https://doi.org/10.1029/2011GB004095, https://agupubs.onlinelibrary.wiley.com/doi/abs/10.1029/2011GB004095, 2012.

Lewis, E. and Wallace, D. W. R.: Program Developed for CO_2 System Calculations, ORNL/CDIAC-105. Carbon Dioxide Information Analysis Center, Oak Ridge National Laboratory, US Department of Energy, Oak Ridge, Tennessee., 1998.

Long, M. C., Lindsay, K., Peacock, S., Moore, J. K., and Doney, S. C.: Twentieth-century oceanic carbon uptake and storage in CESM1(BGC), J. Climate, 26, 6775–6800, https://doi.org/http://dx.doi.org/10.1175/JCLI-D-12-00184.1, 2013.

Lovenduski, N. S., Gruber, N., Doney, S. C., and Lima, I. D.: Enhanced CO2 outgassing in the Southern Ocean from a positive phase of the Southern Annular Mode, Global Biogeochemical Cycles, 21, https://doi.org/https://doi.org/10.1029/2006GB002900, https://agupubs.onlinelibrary.wiley.com/doi/abs/10.1029/2006GB002900, 2007.

Lueker, T. J., Dickson, A. G., and Keeling, C. D.: Ocean pCO_2 calculated from dissolved inorganic carbon, alkalinity, and equations for K1 and K2: validation based on laboratory measurements of CO_2 in gas and seawater at equilibrium, Marine Chemistry, 70, 105 – 119, https://doi.org/https://doi.org/10.1016/S0304-4203(00)00022-0, http://www.sciencedirect.com/science/article/pii/S0304420300000220, 2000.

Maier-Reimer, E., Kriest, I., Segschneider, J., and Wetzel, P.: The HAMburg Ocean Carbon Cycle Model HAMOCC5.1 - Technical Description Release 1.1.Berichte zur Erdsystemforschung, 14., Tech. rep., 2005.

Malmberg, S. A. and Désert, J.: Hydrographic conditions in North Icelandic waters and annual air temperature in Iceland, ICES CM 1999/LM:14,21pp, 1999.

Manno, C., Bednaršek, N., Tarling, G. A., Peck, V. L., Comeau, S., Adhikari, D., Bakker, D. C., Bauerfeind, E., Bergan, A. J., Berning, M. I., Buitenhuis, E., Burridge, A. K., Chierici, M., Flöter, S., Fransson, A., Gardner, J., Howes, E. L., Keul, N., Kimoto, K., Kohnert, P., Lawson, G. L., Lischka, S., Maas, A., Mekkes, L., Oakes, R. L., Pebody, C., Peijnenburg, K. T., Seifert, M., Skinner, J., Thibodeau, P. S., Wall-Palmer, D., and Ziveri, P.: Shelled pteropods in peril: Assessing vulnerability in a high CO2 ocean, Earth-Science Reviews, 169, 132–145, https://doi.org/https://doi.org/10.1016/j.earscirev.2017.04.005, https://www.sciencedirect.com/science/article/pii/S0012825216302495, 2017.

Marcussen, C.; Anderson, L. G.: Discrete profile measurements of carbon dioxide, hydrographic and chemical data during the R/V Oden Lomonosov Ridge off Greenland (LOMROG) expedition (EXPOCODE 77DN20070812) in the Arctic Ocean from 2007-08-12 to 2007-09-19 (NCEI Accession 0170966). NOAA National Centers for Environmental Information., https://doi.org/10.7289/v52n50jb., dataset, 2018.

McCulloch, M., Trotter, J., Montagna, P., Falter, J., Dunbar, R., Freiwald, A., Försterra, G., López Correa, M., Maier, C., Rüggeberg, A., and Taviani, M.: Resilience of cold-water scleractinian corals to ocean acidification: Boron isotopic systematics of pH and saturation state up-regulation, Geochimica et Cosmochimica Acta, 87, 21 – 34, https://doi.org/https://doi.org/10.1016/j.gca.2012.03.027, http://www.sciencedirect.com/science/article/pii/S001670371200169X, 2012.

Meehl, G., Stocker, T., Collins, W., Friedlingstein, P., Gaye, A., Gregory, J., Kitoh, A., Knutti, R., Murphy, J., A. Noda, S. R., I.G. Watterson, A. W., and Zhao, Z.-C.: Global Climate Projections. In: Climate Change 2007: The Physical Science Basis. Contribution of Working Group I to the Fourth Assessment Report of the Intergovernmental Panel on Climate Change [Solomon, S., D. Qin, M. Manning, Z. Chen, M. Marquis, K.B. Averyt, M. Tignor and H.L. Miller (eds.)]. Cambridge University Press, Cambridge, United Kingdom and New York, NY, USA., 2007.

Meinshausen, M., Smith, S. J., Calvin, K., Daniel, J. S., Kainuma, M. L. T., Lamarque, J.-F., Matsumoto, K., Montzka, S. A., Raper, S. C. B., Riahi, K., Thomson, A., Velders, G. J. M., and van Vuuren, D. P. P.: The RCP greenhouse gas concentrations and their extensions from 1765 to 2300, Climatic Change, 109, 213, https://doi.org/10.1007/s10584-011-0156-z, https://doi.org/10.1007/s10584-011-0156-z, 2011.

Messias, M.-J., Watson, A., Johannessen, T., Oliver, K., Olsson, K., Fogelqvist, E., Olafsson, J., Bacon, S., Balle, J., Bergman, N., Budéus, G., Danielsen, M., Gascard, J.-C., Jeansson, E., Olafsdottir, S., Simonsen, K., Tanhua, T., Van Scoy, K., and Ledwell, J.: The Greenland Sea tracer experiment 1996–2002: Horizontal mixing and transport of Greenland Sea Intermediate Water, Progress in Oceanography, 78, 85 – 105, https://doi.org/https://doi.org/10.1016/j.pocean.2007.06.005, http://www.sciencedirect.com/science/article/pii/S0079661108000852, 2008.

Metzl, N., Corbière, A., Reverdin, G., Lenton, A., Takahashi, T., Olsen, A., Johannessen, T., Pierrot, D., Wanninkhof, R., Ólafsdóttir, S. R., Olafsson, J., and Ramonet, M.: Recent acceleration of the sea surface fCO_2 growth rate in the North Atlantic subpolar gyre (1993–2008) revealed by winter observations, Global Biogeochemical Cycles, 24, https://doi.org/10.1029/2009GB003658, https://agupubs.onlinelibrary.wiley.com/doi/abs/10.1029/2009GB003658, 2010.

Middelburg, J. J., Soetaert, K., and Hagens, M.: Ocean Alkalinity, Buffering and Biogeochemical Processes, Reviews of Geophysics, 58, e2019RG000681, https://doi.org/https://doi.org/10.1029/2019RG000681, https://agupubs.onlinelibrary.wiley.com/doi/abs/10.1029/2019RG000681, e2019RG000681 2019RG000681, 2020.

NOAA National Geophysical Data Center: ETOPO1 1 Arc-Minute Global Relief Model. NOAA National Centers for Environmental Information., doi:10.7289/V5C8276M, dataset, 2020.

Nondal, G., Bellerby, R. G. J., Olsen, A., Johannessen, T., and Olafsson, J.: Optimal evaluation of the surface ocean CO2 system in the northern North Atlantic using data from voluntary observing ships, Limnology and Oceanography: Methods, 7, 109–118, https://doi.org/https://doi.org/10.4319/lom.2009.7.109, https://aslopubs.onlinelibrary.wiley.com/doi/abs/10.4319/lom.2009.7.109, 2009.

Ólafsdóttir, S. R., Benoit-Cattin, A., and Danielsen, M.: Dissolved inorganic carbon (DIC), total alkalinity, temperature, salinity, nutrients and dissolved oxygen collected from discrete samples and profile observations during the R/Vs Arni Fridriksson and Bjarni Saemundsson time series IcelandSea (LN6) cruises in the North Atlantic Ocean from 2014-02-18 to 2019-10-31 (NCEI Accession 0209074), https://doi.org/10.25921/qhed-3h84, dataset, 2020.

Ólafsson, J.: Winter mixed layer nutrients in the Irminger and Iceland Seas,1990-2000, ICES Marine Science Symposia, 219, 2003.

Ólafsson, J.: Partial pressure (or fugacity) of carbon dioxide, dissolved inorganic carbon, temperature, salinity and other variables collected from discrete samples, profile and time series profile observations during the R/Vs Arni Fridriksson and Bjarni Saemundsson time series IcelandSea (LN6) cruises in the North Atlantic Ocean from 1985-02-22 to 2013-11-26 (NCEI Accession 0100063), https://doi.org/10.3334/cdiac/otg.carina_icelandsea, dataset, 2012.

Ólafsson, J., Ólafsdóttir, S., Benoit-Cattin, A., Danielsen, M., Arnarson, T. S., and Takahashi, T.: Rate of Iceland Sea acidification from time series measurements, Biogeosciences, 6, 2661–2668, 2009.

Ólafsson, J., Lee, K., Ólafsdóttir, S. R., Benoit-Cattin, A., Lee, C.-H., and Kim, M.: Boron to salinity ratios for Atlantic, Arctic and Polar Waters: A view from downstream, Marine Chemistry, 224, 103 809, https://doi.org/https://doi.org/10.1016/j.marchem.2020.103809, http://www.sciencedirect.com/science/article/pii/S0304420320300633, 2020a.

Ólafsson, J., Ólafsdóttir, S. R., Takahashi, T., Danielsen, M., and Arnarson, T. S.: Enhancement of the North Atlantic CO_2 sink by Arctic Waters, Biogeosciences Discussions, 2020, 1–21, https://doi.org/10.5194/bg-2020-313, https://bg.copernicus.org/preprints/bg-2020-313/, 2020b.

Olsen, A. and Omar, A. M.: Dissolved inorganic carbon, alkalinity, temperature, salinity and other variables collected from discrete sample and profile observations using Alkalinity titrator, CTD and other instruments from the G.O. SARS in the North Greenland Sea and Norwegian Sea from 2006-07-21 to 2006-08-05 (NCEI Accession 0105859). NOAA National Centers for Environmental Information., https://doi.org/10.3334/cdiac/otg.clivar_75n_2006, dataset, 2013.

Olsen, A., Omar, A. M., Bellerby, R. G. J., Johannessen, T., Ninnemann, U., Brown, K. R., Olsson, K. A., Olafsson, J., Nondal, G., Kivimäe, C., Kringstad, S., Neill, C., and Olafsdottir, S.: Magnitude and origin of the anthropogenic CO_2 increase and 13C Suess effect in the Nordic seas since 1981, Global Biogeochemical Cycles, 20, https://doi.org/10.1029/2005GB002669, https://agupubs.onlinelibrary.wiley.com/doi/abs/10.1029/2005GB002669, 2006.

Olsen, A., Omar, A. M., and Johannessen, T.: Dissolved inorganic carbon, alkalinity, temperature, salinity and other variables collected from discrete sample and profile observations using CTD, bottle and other instruments from the HAKON MOSBY in the North Atlantic Ocean, North Greenland Sea and Norwegian Sea from 2001-05-27 to 2001-06-19 (NCEI Accession 0113754). NOAA National Centers for Environmental Information., https://doi.org/10.3334/cdiac/otg.carina_58aa20010527, dataset, 2013.

Olsen, A., Lange, N., Key, R. M., Tanhua, T., Álvarez, M., Becker, S., Bittig, H. C., Carter, B. R., Cotrim da Cunha, L., Feely, R. A., van Heuven, S., Hoppema, M., Ishii, M., Jeansson, E., Jones, S. D., Jutterström, S., Karlsen, M. K., Kozyr, A., Lauvset, S. K., Lo Monaco, C., Murata, A., Pérez, F. F., Pfeil, B., Schirnick, C., Steinfeldt, R., Suzuki, T., Telszewski, M., Tilbrook, B., Velo, A., and Wanninkhof, R.: GLODAPv2.2019 – an update of GLODAPv2, Earth System Science Data, 11, 1437–1461, https://doi.org/10.5194/essd-11-1437-2019, https://essd.copernicus.org/articles/11/1437/2019/, 2019.

Omar, A. M. and Olsen, A.: Dissolved inorganic carbon, alkalinity, temperature, salinity and other variables collected from discrete sample and profile observations using CTD, bottle and other instruments from the HAKON MOSBY in the Barents Sea, North Greenland Sea and Norwegian Sea from 1999-10-03 to 1999-10-11 (NCEI Accession 0113888). NOAA National Centers for Environmental Information., https://doi.org/10.3334/cdiac/otg.carina_58aa19991003., dataset, 2013.

Omar, A. M. and Skogseth, R.: Dissolved inorganic carbon, alkalinity, temperature, salinity and other variables collected from discrete sample and profile observations using CTD, bottle and other instruments from the HAKON MOSBY in the Barents Sea and Norwegian Sea from 2001-08-22 to 2001-08-29 (NCEI Accession 0113887). NOAA National Centers for Environmental Information., https://doi.org/10.3334/cdiac/otg.carina_58aa20010822, dataset, 2013.

Omar, Abdirahman M.; Østerhus, S.: Dissolved inorganic carbon, alkalinity, temperature, salinity and other variables collected from discrete sample and profile observations using CTD, bottle and other instruments from the HAKON MOSBY in the Barents Sea from 2000-09-23 to 2000-10-03 (NCEI Accession 0113886). NOAA National Centers for Environmental Information, https://doi.org/10.3334/cdiac/otg.carina_58aa20000923, dataset, 2013.

Orr, J. C.: Recent and future changes in ocean carbonate chemistry, In Ocean Acidification, ed. J-P Gattuso, L Hansson, pp. 41–66, Oxford University Press, Oxford, UK, 2011.

Orr, J. C., Fabry, V. J., Aumont, O., Bopp, L., Doney, S. C., Feely, R. A., Gnanadesikan, A., Gruber, N., Ishida, A., Joos, F., Key, R. M., Lindsay, K., Maier-Reimer, E., Matear, R., Monfray, P., Mouchet, A., Najjar, R. G., Plattner, G.-K., Rodgers, K. B., Sabine, C. L., Sarmiento, J. L., Schlitzer, R., Slater, R. D., Totterdell, I. J., Weirig, M.-F., Yamanaka, Y., and Yool, A.: Anthropogenic ocean acidification over the twenty-first century and its impact on calcifying organisms, Nature, 437, 681–686, https://doi.org/10.1038/nature04095, https://doi.org/10.1038/nature04095, 2005.

Orr, J. C., Epitalon, J.-M., Dickson, A. G., and Gattuso, J.-P.: Routine uncertainty propagation for the marine carbon dioxide system, Marine Chemistry, 207, 84–107, https://doi.org/https://doi.org/10.1016/j.marchem.2018.10.006, https://www.sciencedirect.com/science/article/pii/S030442031830149X, 2018.

Østerhus, S. and Gammelsrød, T.: The Abyss of the Nordic Seas Is Warming, Journal of Climate, 12, 3297–3304, https://doi.org/10.1175/1520-0442(1999)012<3297:TAOTNS>2.0.CO;2, https://doi.org/10.1175/1520-0442(1999)012<3297:TAOTNS>2.0.CO;2, 1999.

Oziel, L., Baudena, A., Ardyna, M., Massicotte, P., Randelhoff, A., Sallée, J.-B., Ingvaldsen, R. B., Devred, E., and Babin, M.: Faster Atlantic currents drive poleward expansion of temperate phytoplankton in the Arctic Ocean, Nature Communications, 11, 1705, https://doi.org/10.1038/s41467-020-15485-5, https://doi.org/10.1038/s41467-020-15485-5, 2020.

Pegler, K., Graf, G., and Pfannkuche, O.: Partial pressure (or fugacity) of carbon dioxide, dissolved inorganic carbon, alkalinity, temperature, salinity and other variables collected from discrete sample and profile observations using CTD, bottle and other instruments from the METEOR in the North Atlantic Ocean, North Greenland Sea and Norwegian Sea from 1992-07-01 to 1992-08-31 (NCEI Accession 0113985). NOAA National Centers for Environmental Information., https://doi.org/10.3334/cdiac/otg.carina_06mt19920701, dataset, 2013.

Perez, F. F., Fontela, M., García-Ibáñez, M. I., Mercier, H., Velo, A., Lherminier, P., Zunino, P., de la Paz, M., Alonso-Pérez, F., Guallart, E. F., and Padin, X. A.: Meridional overturning circulation conveys fast acidification to the deep Atlantic Ocean, Nature, 554, 515–518, https://doi.org/10.1038/nature25493, https://doi.org/10.1038/nature25493, 2018.

Pérez, F. F., Olafsson, J., Ólafsdóttir, S. R., Fontela, M., and Takahashi, T.: Contrasting drivers and trends of ocean acidification in the subarctic Atlantic, Scientific Reports, 11, 13 991, https://doi.org/10.1038/s41598-021-93324-3, https://doi.org/10.1038/s41598-021-93324-3, 2021.

Raven, J., Caldeira, K., Elderfield, H., Hoegh-Guldberg, O., Liss, P., Riebesell, U., Shepherd, J., Turley, C., and Watson, A.: Ocean acidification due to increasing atmospheric carbon dioxide, Policy document, The Royal Society, London Pp. 1–68, 2005.

Ruiz-Barradas, A., Chafik, L., Nigam, S., and Häkkinen, S.: Recent subsurface North Atlantic cooling trend in context of Atlantic decadal-to-multidecadal variability, Tellus A: Dynamic Meteorology and Oceanography, 70, 1–19, https://doi.org/10.1080/16000870.2018.1481688, https://doi.org/10.1080/16000870.2018.1481688, 2018.

Sarmiento, J. L. and Gruber, N.: Ocean Biogeochemical Dynamics, chap. 8, pp. 318–358, Princeton University Press, Princeton, Woodstock, 2006.

Schauer, U., Jones, E. M., Ulfsbo, A., Hansell, D. A., Smethie, William M., J., Rabe, B., and van Ooijen, J. C.: Discrete, profile measurements of the dissolved inorganic carbon (DIC), total alkalinity, pH on total scale and other hydrographic and chemical data obtained during the PS-94, ARK-XXIX/3, TransArc-II cruise onboard the R/V Polarstern (EXPOCODE 06AQ20150817) in the central Arctic Ocean from 2015-08-17 to 2015-10-15 (NCEI Accession 0170256). NOAA National Centers for Environmental Information., https://doi.org/10.7289/v5319t5z, dataset, 2018.

Shu, Q., Qiao, F., Song, Z., Zhao, J., and Li, X.: Projected Freshening of the Arctic Ocean in the 21st Century, Journal of Geophysical Research: Oceans, 123, 9232–9244, https://doi.org/10.1029/2018JC014036, https://agupubs.onlinelibrary.wiley.com/doi/abs/10.1029/2018JC014036, 2018.

Skjelvan, I., Falck, E., Rey, F., and Kringstad, S. B.: Inorganic carbon time series at Ocean Weather Station M in the Norwegian Sea, Biogeosciences, 5, 549–560, https://doi.org/10.5194/bg-5-549-2008, https://bg.copernicus.org/articles/5/549/2008/, 2008.

Skjelvan, I., Johannessen, T., and Anderson, L. G.: Dissolved inorganic carbon, alkalinity, temperature, salinity and other variables collected from discrete sample and profile observations using CTD, bottle and other instruments from the HAKON MOSBY in the North Greenland Sea and Norwegian Sea from 1994-02-24 to 1994-03-17 (NCEI Accession 0113541). NOAA National Centers for Environmental Information. Dataset., https://doi.org/10.3334/cdiac/otg.carina_58aa19940224, dataset, 2013.

Skjelvan, I., Jeansson, E., Chierici, M., Omar, A., Olsen, A., Lauvset, S., and Johannessen, T.: Havforsuring og opptak av antropogent karbon i de Nordiske hav [Ocean acidification and uptake of anthropogenic carbon in the Nordic Seas], 1981-2013. Miljødirektoratet, Rapport M244-2014, Tech. rep., 2014.

Skjelvan, I., Jones, E., Chierici, M., Frigstad, H., Børsheim, K., Lødemel, H., Kutti, T., King, A., Sørensen, K., Omar, A., Bellerby, R., Christensen, G., Marty, S., Protsenko, E., Mengeot, C., Valestrand, L., Norli, M., Jackson-Misje, K., Apelthun, L., de Lange, T., Johannessen, T., and Mourgues., C.: Monitoring of the ocean acidification in Norwegian seas in 2020, Report, Miljødirektoratet, M-2056, Tech. rep., 2021.

Skogen, M. D., Olsen, A., Børsheim, K. Y., Sandø, A. B., and Skjelvan, I.: Modelling ocean acidification in the Nordic and Barents Seas in present and future climate, Journal of Marine Systems, 131, 10–20, https://doi.org/https://doi.org/10.1016/j.jmarsys.2013.10.005, https://www.sciencedirect.com/science/article/pii/S092479631300211X, 2014.

Skogen, M. D., Hjøllo, S. S., Sandø, A. B., and Tjiputra, J.: Future ecosystem changes in the Northeast Atlantic: a comparison between a global and a regional model system, ICES Journal of Marine Science, 75, 2355–2369, https://doi.org/10.1093/icesjms/fsy088, https://doi.org/10.1093/icesjms/fsy088, 2018.

Somavilla, R., Schauer, U., and Budéus, G.: Increasing amount of Arctic Ocean deep waters in the Greenland Sea, Geophysical Research Letters, 40, 4361–4366, https://doi.org/10.1002/grl.50775, https://agupubs.onlinelibrary.wiley.com/doi/abs/10.1002/grl.50775, 2013.

Stöven, T., Tanhua, T., Hoppema, M., and von Appen, W.-J.: Transient tracer distributions in the Fram Strait in 2012 and inferred anthropogenic carbon content and transport, Ocean Science, 12, 319–333, https://doi.org/10.5194/os-12-319-2016, https://os.copernicus.org/articles/12/319/2016/, 2016.

Takahashi, T., Olafsson, J., Goddard, J. G., Chipman, D. W., and Sutherland, S. C.: Seasonal variation of CO_2 and nutrients in the high-latitude surface oceans: A comparative study, Global Biogeochemical Cycles, 7, 843–878, https://doi.org/10.1029/93GB02263, https://agupubs.onlinelibrary.wiley.com/doi/abs/10.1029/93GB02263, 1993.

Takahashi, T., Sutherland, S. C., Sweeney, C., Poisson, A., Metzl, N., Tilbrook, B., Bates, N., Wanninkhof, R., Feely, R. A., Sabine, C., Olafsson, J., and Nojiri, Y.: Global sea–air CO2 flux based on climatological surface ocean pCO2, and seasonal biological and temperature effects, Deep Sea Research Part II: Topical Studies in Oceanography, 49, 1601–1622, https://doi.org/https://doi.org/10.1016/S0967-

0645(02)00003-6, https://www.sciencedirect.com/science/article/pii/S0967064502000036, the Southern Ocean I: Climatic Changes in the Cycle of Carbon in the Southern Ocean, 2002.

Tanhua, Toste; Hoppema, M.: Dissolved Inorganic Carbon (DIC), Total Alkalinity, Oxygen and other Hydrographic and Chemical Data Obtained During the R/V Polarstern Cruise ARKXXVII/1 (EXPOCODE 06AQ20120614) along the CLIVAR Repeat Section 75N in the North Atlantic Ocean from 2012-06-14 to 2012-07-15 (NCEI Accession 0162432). NOAA National Centers for Environmental Information., dataset, 2017.

Taylor, K. E., Stouffer, R. J., and Meehl, G. A.: An Overview of CMIP5 and the Experiment Design, Bulletin of the American Meteorological Society, 93, 485–498, https://doi.org/10.1175/BAMS-D-11-00094.1, https://doi.org/10.1175/BAMS-D-11-00094.1, 2012.

Terhaar, J., Kwiatkowski, L., and Bopp, L.: Emergent constraint on Arctic Ocean acidification in the twenty-first century, Nature, 582, 379–383, https://doi.org/10.1038/s41586-020-2360-3, https://doi.org/10.1038/s41586-020-2360-3, 2020a.

Terhaar, J., Tanhua, T., Stöven, T., Orr, J. C., and Bopp, L.: Evaluation of Data-Based Estimates of Anthropogenic Carbon in the Arctic Ocean, Journal of Geophysical Research: Oceans, 125, e2020JC016 124, https://doi.org/https://doi.org/10.1029/2020JC016124, https://agupubs.onlinelibrary.wiley.com/doi/abs/10.1029/2020JC016124, e2020JC016124 10.1029/2020JC016124, 2020b.

Terhaar, J., Torres, O., Bourgeois, T., and Kwiatkowski, L.: Arctic Ocean acidification over the 21st century co-driven by anthropogenic carbon increases and freshening in the CMIP6 model ensemble, Biogeosciences, 18, 2221–2240, https://doi.org/10.5194/bg-18-2221-2021, https://bg.copernicus.org/articles/18/2221/2021/, 2021.

Tjiputra, J. F., Assmann, K., and Heinze, C.: Anthropogenic carbon dynamics in the changing ocean, Ocean Science, 6, 605–614, https://doi.org/10.5194/os-6-605-2010, https://os.copernicus.org/articles/6/605/2010/, 2010.

Tjiputra, J. F., Roelandt, C., Bentsen, M., Lawrence, D. M., Lorentzen, T., Schwinger, J., Seland, Ø., and Heinze, C.: Evaluation of the carbon cycle components in the Norwegian Earth System Model (NorESM), Geoscientific Model Development, 6, 301–325, https://doi.org/10.5194/gmd-6-301-2013, https://gmd.copernicus.org/articles/6/301/2013/, 2013.

Tjiputra, J. F., Grini, A., and Lee, H.: Impact of idealized future stratospheric aerosol injection on the large-scale ocean and land carbon cycles, Journal of Geophysical Research: Biogeosciences, 121, 2–27, https://doi.org/https://doi.org/10.1002/2015JG003045, https://agupubs.onlinelibrary.wiley.com/doi/abs/10.1002/2015JG003045, 2016.

Turley, C. M., Roberts, J. M., and Guinotte, J. M.: Corals in deep-water: will the unseen hand of ocean acidification destroy cold-water ecosystems?, Coral Reefs, 26, 445–448, https://doi.org/10.1007/s00338-007-0247-5, https://doi.org/10.1007/s00338-007-0247-5, 2007.

Uppström, L. R.: The boron/chlorinity ratio of deep-sea water from the Pacific Ocean, Deep Sea Research and Oceanographic Abstracts, 21, 161 – 162, https://doi.org/https://doi.org/10.1016/0011-7471(74)90074-6, http://www.sciencedirect.com/science/article/pii/0011747174900746, 1974.

van Heuven, S., Pierrot, D., Rae, J., Lewis, E., and Wallace, D.: MATLAB Program Developed for CO_2 System Calculations, ORNL/CDIAC-105b. Carbon Dioxide Information Analysis Center, Oak Ridge National Laboratory, US Department of Energy, Oak Ridge, Tennessee., 2011.

van Vuuren, D. P., Edmonds, J., Kainuma, M., Riahi, K., Thomson, A., Hibbard, K., Hurtt, G. C., Kram, T., Krey, V., Lamarque, J.-F., Masui, T., Meinshausen, M., Nakicenovic, N., Smith, S. J., and Rose, S. K.: The representative concentration pathways: an overview, Climatic Change, 109, 5, https://doi.org/10.1007/s10584-011-0148-z, https://doi.org/10.1007/s10584-011-0148-z, 2011a.

van Vuuren, D. P., Stehfest, E., den Elzen, M. G. J., Kram, T., van Vliet, J., Deetman, S., Isaac, M., Klein Goldewijk, K., Hof, A., Mendoza Beltran, A., Oostenrijk, R., and van Ruijven, B.: RCP2.6: exploring the possibility to keep global mean temperature increase below 2°C, Climatic Change, 109, 95, https://doi.org/10.1007/s10584-011-0152-3, https://doi.org/10.1007/s10584-011-0152-3, 2011b.

Våge, K., Pickart, R. S., Spall, M. A., Moore, G., Valdimarsson, H., Torres, D. J., Erofeeva, S. Y., and Nilsen, J. E. Ø.: Revised circulation scheme north of the Denmark Strait, Deep Sea Research Part I: Oceanographic Research Papers, 79, 20 – 39, https://doi.org/https://doi.org/10.1016/j.dsr.2013.05.007, http://www.sciencedirect.com/science/article/pii/S0967063713001040, 2013.

Våge, K., Moore, G., Jónsson, S., and Valdimarsson, H.: Water mass transformation in the Iceland Sea, Deep Sea Research Part I: Oceanographic Research Papers, 101, 98 – 109, https://doi.org/https://doi.org/10.1016/j.dsr.2015.04.001, http://www.sciencedirect.com/science/article/pii/S0967063715000680, 2015.

Wallace, D. W. R. and Deming, J.: Dissolved inorganic carbon, alkalinity, temperature, salinity and other variables collected from discrete sample and profile observations using CTD, bottle and other instruments from the USCGC POLAR SEA in the North Greenland Sea from 1992-07-15 to 1992-08-14 (NCEI Accession 0115687). NOAA National Centers for Environmental Information., https://doi.org/10.3334/cdiac/otg.carina_32l919920715, dataset, 2014.

Woosley, R. J. and Millero, F. J.: Freshening of the western Arctic negates anthropogenic carbon uptake potential, Limnology and Oceanography, 65, 1834–1846, https://doi.org/https://doi.org/10.1002/lno.11421, https://aslopubs.onlinelibrary.wiley.com/doi/abs/10.1002/lno.11421, 2020.

Wu, Y., Hain, M. P., Humphreys, M. P., Hartman, S., and Tyrrell, T.: What drives the latitudinal gradient in open-ocean surface dissolved inorganic carbon concentration?, Biogeosciences, 16, 2661–2681, https://doi.org/10.5194/bg-16-2661-2019, https://bg.copernicus.org/articles/16/2661/2019/, 2019.

Yukimoto, S., Yoshimura, H., and Hosaka, M.: Meteorological Research Institute-Earth System Model v1 (MRI-ESM1)—Model Description.Technical Report of MRI. Ibaraki, Japan, 88 pp., Tech. rep., 2011.

Zeebe, R. and Wolf-Gladrow, D.: CO_2 in Seawater: Equilibrium, Kinetics, Isotopes, vol. 65 of *Elsevier Oceanography Series*, Elsevier Science, 1 edn., 2001.

Zheng, M.-D. and Cao, L.: Simulation of global ocean acidification and chemical habitats of shallow- and cold-water coral reefs, Advances in Climate Change Research, 5, 189–196, https://doi.org/https://doi.org/10.1016/j.accre.2015.05.002, https://www.sciencedirect.com/science/article/pii/S1674927815000210, including special topic on China's carbon emissions peaking, 2014.